Molecular Therapy
Methods & Clinical Development
Original Article

Efficient nonviral integration of large transgenes into human T cells using Cas9-CLIPT

Anna Tommasi,[1,2,8] Dan Cappabianca,[1,2,8] Madison Bugel,[1,2] Kirstan Gimse,[1] Karl Lund-Peterson,[4] Hum Shrestha,[4] Denis Arutyunov,[4] James A. Williams,[4] Seshidhar Reddy Police,[4] Venkata Indurthi,[4] Sage Z. Davis,[6] Muhammed Murtaza,[6,7] Christian M. Capitini,[3,5] and Krishanu Saha[1,2,3,5]

[1]Wisconsin Institute for Discovery, University of Wisconsin-Madison, Madison, WI 53715, USA; [2]Department of Biomedical Engineering, University of Wisconsin-Madison, Madison, WI 53715, USA; [3]University of Wisconsin Carbone Cancer Center, University of Wisconsin-Madison, Madison, WI 53705, USA; [4]Aldevron, Fargo, ND 58104, USA; [5]Department of Pediatrics, University of Wisconsin School of Medicine and Public Health, Madison, WI 53705, USA; [6]Center for Human Genomics and Precision Medicine, University of Wisconsin-Madison, Madison, WI 53705 USA; [7]Department of Surgery, University of Wisconsin-Madison, Madison, WI 53705, USA

CRISPR-Cas9 ribonucleoproteins (RNPs) combined with a nucleic acid template encoding a chimeric antigen receptor (CAR) transgene can edit human cells to produce CAR T cells with precise CAR insertion at a single locus. However, many human cells have adverse innate immune responses to foreign nucleic acids, particularly circular double-stranded DNA (dsDNA). Here, we introduce Cleaved, LInearized with Protein Template (Cas9-CLIPT), a circular plasmid containing a single target sequence for the Cas9 RNP, such that during manufacturing, Cas9-RNP binds and cleaves the plasmid to linearize the dsDNA *in vitro*. Cas9-RNP remains bound to the linearized template and is delivered to cells to promote precise knock-in via homology-directed repair with Cas9-CLIPT. Cas9-CLIPT Nanoplasmids generate up to 1.7-fold higher rates of precise knock-in relative to linearized dsDNA, reaching efficiencies up to 60% with non-homologous end joining inhibition. Cas9-CLIPT-manufactured GD2 *TRAC*-CAR T cells are potent against GD2$^+$ neuroblastoma cells and exhibit an enriched stem cell memory phenotype. On several electroporation instruments and approaching clinically relevant yields, we successfully manufactured *TRAC*-CAR T cells using Cas9-CLIPT plasmids containing large (2–6 kb) transgenes. Cas9-CLIPT strategies have the potential to simplify donor template production and integrate large transgenes, allowing for more efficient nonviral manufacturing of multifunctional, genome-edited immune cell therapies.

INTRODUCTION

Seven available US Food and Drug Administration (FDA) approved chimeric antigen receptor (CAR) T cell therapies against hematologic malignancies[1,2] and one FDA approval for an MAGE-A4 T cell receptor (TCR)-edited T cell therapy[3] against synovial sarcoma demonstrate the promise of engineering primary T cells to advance human health. However, current techniques to manufacture autologous genetically engineered T cells are limited by manufacturing time, cost, and occasional manufacturing failure. The first approved CAR T product, tisagenlecleucel, takes 3–4 weeks from leukapheresis to re-infusion[4,5] of ∼0.1–10 billion therapeutic cells per patient to complete one dose of CAR T cell therapy.[6] Further, CAR T cell clinical manufacturing processes report manufacturing failure rates from 1% to 13%.[7] To be eligible to receive CAR T cell therapy, patients must have already exhausted alternative lifesaving treatments like chemotherapy or hematopoietic stem cell transplant that could not cure their cancer.[8,9] Thus, there is an alarming need to optimize CAR T manufacturing processes to expedite manufacturing, prevent manufacturing failure, and reduce costs. With an ongoing debate on whether there is a risk of secondary malignancy from virally transduced T cells,[10] non-viral delivery of CAR transgenes is increasingly being explored.[11,12]

CRISPR-Cas9 genome editing has emerged as an alternative to viral transduction of T cells. Short guide RNA (gRNA) sequences can complex with Cas9 nuclease to form a ribonucleoprotein (RNP) capable of producing double-strand breaks (DSBs) at a targeted location in the genome. These DSBs are repaired via error-prone, non-homologous end joining (NHEJ) to knock genes out or homology-directed repair (HDR) to incorporate exogenous DNA.[13,14] While the CAR transgene has been incorporated successfully at multiple loci (*TRAC*, *PDCD1*, and *B2M*)[15,16] in human cells, transgene integration specifically upstream of the endogenous T cell receptor, alpha chain (*TRAC*) promoter produces *TRAC*-CAR T cells with a stem cell memory-like phenotype that are more resistant to exhaustion. A more stem

Received 17 June 2024; accepted 17 February 2025;
https://doi.org/10.1016/j.omtm.2025.101437.

[8]These authors contributed equally

Correspondence: Krishanu Saha, Wisconsin Institute for Discovery, University of Wisconsin-Madison, Madison, WI 53715, USA.
E-mail: ksaha@wisc.edu

Published by Elsevier Inc. on behalf of The American Society of Gene and Cell Therapy.
This is an open access article under the CC BY-NC-ND license (http://creativecommons.org/licenses/by-nc-nd/4.0/).

cell-like CAR T cell product is correlated to increased persistence *in vivo*, which is beneficial for targeting hematologic malignancies and solid tumors.[17–19]

TRAC-CAR T cell manufacturing historically has relied on viral vectors or linear, double-stranded DNA (dsDNA) HDR donor templates generated via polymerase chain reaction (PCR).[15–17] Often, restriction enzyme digestions paired with DNA purification methods, such as magnetic solid-phase reversible immobilization (SPRI) beads, are used to linearize donor DNA templates, which is time-consuming, expensive, and reduces donor DNA template yield.[17,18] PCR amplification with high-fidelity polymerases, unfortunately, has also resulted in inconsistent product quality and has been challenging to scale up,[20,21] creating a bottleneck in translational work and deployment of early-phase clinical trials. dsDNA templates often result in high cell toxicity and low knock-in efficiencies, especially with templates >1.5 kb, which ultimately limits CAR T cell yields.[18,22,23] Given the large number of therapeutic cells needed to see benefits *in vivo*, any setback to CAR T cell yields can be detrimental to clinical trials. For example, a recent phase 1 clinical trial for a CRISPR-Cas9 manufactured CD19 CAR at the *PDCD1* locus for relapsed/refractory B cell non-Hodgkin's lymphoma failed to produce enough cells for three out of eight patients.[24]

One alternative approach to using dsDNA HDR templates for the CAR transgene includes linear single-stranded DNAs (ssDNA). CAR T cell products manufactured with these templates include a truncated Cas9 target sequence (tCTS) to improve T cell knock-in and viability[25] relative to templates without tCTS. RNP binding to an ssDNA template has been shown to enhance the trafficking of the template due to the nuclear localization signal (NLS) on the Cas9 protein.[26] One study found an improvement in knock-in efficiencies of a CAR transgene when using tCTS-modified ssDNA compared to dsDNA and tCTS-modified dsDNA.[25] However, ssDNA is prone to cytidine deamination by APOBEC-AID deaminases.[27] Base substitution mutations have been observed in genomic DNA through Cas9-generated DSBs repaired with ssDNA via HDR, resulting in imprecise encoding of the intended transgene within the genome.[27] Fewer base substitution mutations were observed in cells edited with dsDNA templates compared to ssDNA templates.[27] Further, plasmid DNA is simple to produce and stable in circular form, making it easier to store and transport than ssDNA.[28] Scalable dsDNA HDR templates can either be produced with conventional plasmid backbones or the Nanoplasmid platform specifically designed for antibiotic-free manufacturing of plasmid DNA.[28,29] Nanoplasmid backbones include two components: a small (∼300 bp) R6K origin of replication and RNA-OUT cassette (∼70 bp). The latter encodes an antisense RNA that enables an antibiotic-free selection of *Escherichia coli* cells in the presence of sucrose by preventing the expression of genome-integrated levansucrase gene *sacB* and production of the toxic oligosaccharides from sucrose.[29] Nanoplasmids can be produced in mass quantities under Good Manufacturing Practice (GMP) conditions and therefore used in clinical trials as a vector or as an ancillary material for CAR T cell production.[30–32] Nanoplasmids are smaller than traditional plasmids due to their small (<500 bp) backbone and can improve *TRAC*-CAR T cell yields 2- to 3-fold relative to traditional pUC plasmids and linear dsDNA when used as an HDR donor template.[23] In addition, having minimal bacterial backbone reduces transgene silencing after genomic insertion.[33]

In an attempt to eliminate DNA template manufacturing bottlenecks, gRNA target sequences have been incorporated into plasmid dsDNA to produce RNP-based linear DNA templates.[22,34,35] Previous studies conducted with these plasmid templates that include gRNA target sequences have shown promise in generating cell therapy products via homology-mediated end joining (HMEJ) transgene knock-in rather than HDR.[22,34,35] These HMEJ cell products exhibit higher cell yields and larger knock-in efficiencies relative to linearized or plasmid donor template cell products.[22,34,35] Specifically, *TRAC*-CAR T cells have been manufactured with Nanoplasmid templates containing either one or two gRNA target sites.[36,37] These approaches exploit NHEJ to insert an anti-GD2 CAR[36] or incorporate two 'universal guide RNA' cut sites separate from the *TRAC* gRNA to integrate an anti-CD19 CAR.[37] However, integration via end joining processes can result in non-targeted insertion. Furthermore, using two separate gRNAs increases manufacturing costs and reduces the available volume in an electroporation (EP) cuvette for RNP and donor template. EP instruments are typically volume-limited, and any volume taken up by a universal gRNA solution reduces the volume of the RNP solution targeting the genomic locus or the HDR template. Within mouse embryonic stem cells, dsDNA HDR donor templates with a single gRNA target site together with transient inhibition of DNA polymerase theta and DNA-protein kinase (PK) boosted HDR integration.[38] Whether similar strategies would benefit CRISPR-Cas9 gene editing in human T cells with different DNA repair mechanisms and innate immune responses to nucleic acids is unknown.

Here, we develop a dsDNA Nanoplasmid template called Cas9-CLIPT (Cleaved, LInearized with Protein Template), that contains a single Cas9 gRNA target sequence and our HDR template to improve knock-in via HDR. This strategy facilitates *in vitro* dsDNA linearization, thereby eliminating the need for restriction enzyme-based linearization. Importantly, the strategy simplifies the amount of necessary gene editing reagents and thus reduces manufacturing time, manufacturing cost, and human error.[34,37] Our Cas9-CLIPT encodes a GD2 CAR that can be used to produce *TRAC*-CAR T cells reaching HDR knock-in efficiencies up to 60%. We demonstrate improved HDR knock-in on several EP instruments, with one instrument at large-scale, relevant for clinical-scale manufacturing. Further, *TRAC*-CAR T cells with a large transgene insertion (5.5 kb) expressing an inducible fluorescence reporter can be generated using Cas9-CLIPT manufacturing workflows. Our Cas9-CLIPT platform can produce high yields of *TRAC*-CAR T cells that maintain a stem cell memory phenotype and potency against solid tumor targets. These advances could streamline non-viral CAR T cell manufacturing to increase CAR T cell yield and simplify cell therapy manufacturing processes.

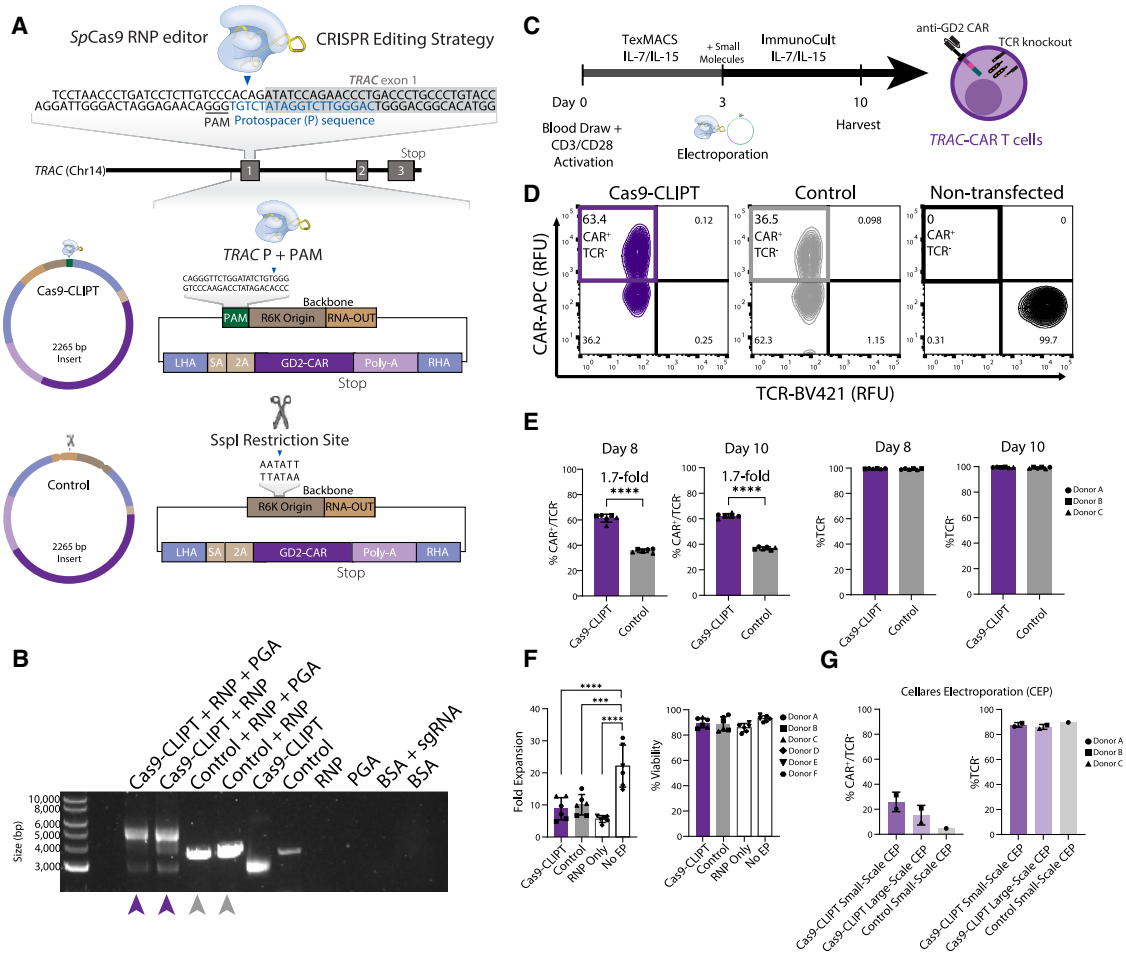

Figure 1. Robust manufacturing of *TRAC*-CAR T cells with Cas9-CLIPT

(A) An *Sp*Cas9 RNP complex targeted to exon 1 of the *TRAC* locus was used to insert dsDNA HDR donor templates containing a GD2 CAR transgene under the control of the endogenous *TRAC* promoter: Cas9-CLIPT and Control template. Cas9-CLIPT contains a *TRAC* gRNA site with PAM to be linearized by the RNP with *TRAC* sgRNA, while the Control template was linearized via an SspI restriction site. (B) Cas9-CLIPT or Control DNA (±PGA) were incubated with RNP for 10 min and run on a 1% agarose gel (lanes 3–6) with a 1-kb plus ladder (lane 1) and controls (lanes 7–12). (C) Isolated T cells were activated with anti-CD3/CD28 beads in TexMACS for 3 days; electroporated with RNP, PGA, and Nanoplasmid donor templates; recovered in ImmunoCult-XF supplemented with IL-7/IL-15 and M3814; and expanded in ImmunoCult-XF supplemented with IL-7/IL-15 until day 10 to manufacture *TRAC*-CAR T cells. (D) Representative contour plots of Cas9-CLIPT, Control *TRAC*-CAR T cells, or non-transfected samples analyzed for CAR and TCR expression on day 8 (day 5 post-EP). (E and F) Bar graphs of Cas9-CLIPT or Control *TRAC*-CAR T cell (E) CAR or TCR expression on days 8 and 10 of manufacturing and (F) fold expansion and viability on day 10 with controls RNP only (T cells electroporated with RNP but not Cas9-CLIPT) and No electroporation (EP) (T cells that were treated with Cas9-CLIPT but were not electroporated). (G) CAR and TCR expression of Cas9-CLIPT and Control *TRAC*-CAR T cells manufactured at small- (5e6 cells) and large- (50e6 cells) scales on the Cellares EP device, without treatment of PGA or M3814. CAR, chimeric antigen receptor; Cas9-CLIPT, cleaved, linearized with protein template; dsDNA, double-stranded DNA; RNP, ribonucleoprotein; *TRAC*, T cell receptor alpha constant. $N_{Cas9\text{-}CLIPT} = N_{Control} = 6$ (3 donors), $N_{RNP\ Only} = N_{No\ EP} = 6$ (3 donors), $N_{Cas9\text{-}CLIPT\ Small\ CEP} = N_{Cas9\text{-}CLIPT\ Large\ CEP} = 2$, $N_{Control\ Small\ CEP} = 1$ (3 separate donors). Error bars represent mean and standard deviation. Statistical significance was determined with paired t-tests; ***$p < 0.001$; ****$p < 0.0001$.

RESULTS

Manufacturing Cas9-CLIPT *TRAC*-CAR T cells

TRAC-CAR T cell manufacturing must yield robust numbers of CAR^+ cells and requires well-characterized manufacturing of ancillary materials to meet GMP requirements.[39,40] We explored whether incorporating a single target sequence consisting of a protospacer sequence (P) together with the protoadjacent motif sequence (PAM) for a *TRAC* single guide RNA (sgRNA) into a Nanoplasmid donor template could streamline non-viral CAR T cell manufacturing. We constructed two different HDR templates containing a GD2 CAR as (1) a circular Cas9-CLIPT template that can be linearized by an RNP with *TRAC* sgRNA and (2) a "Control" circular plasmid that can be linearized via an SspI restriction site (Figure 1A). We chose to insert the P + PAM sequence upstream of the left homology arm in an orientation such that Cas9 cleavage would produce a linearized plasmid, containing the Nanoplasmid backbone

downstream of the right homology arm. In this design, any unintended integration of the backbone through HDR-independent DNA repair would not disrupt the transcription of the CAR.

We prepared the two HDR templates and performed a gel shift assay using RNP, with and without poly-L-glutamic acid (PGA)[26] for both HDR templates. After incubation with RNP for 10 min, regardless of PGA addition, the Cas9-CLIPT Nanoplasmid was linearized (Figure 1B). The Cas9-CLIPT samples migrated slower within the electrophoresis gel, indicating a larger molecular weight for the Cas9-CLIPT molecular complex than the SspI-linearized Control Nanoplasmid. The slow migration depended on the sgRNA sequence, as the Cas9-CLIPT Nanoplasmid incubated with a non-targeting sgRNA RNP failed to migrate slowly (Figure S1). These results indicate that Cas9-CLIPT Nanoplasmid forms a complex with the RNP, based upon the sgRNA sequence, and becomes linearized within minutes of incubation with a matching RNP.

The first time the gel shift assay was performed, the Control Nanoplasmid underwent one freeze/thaw and showed one band of the correct size (Figure S2). After the Control Nanoplasmid and Cas9-CLIPT Nanoplasmid underwent multiple freeze/thaws, another gel shift assay was performed, and two bands were observed for control Nanoplasmid: one at the correct size of the linear Control Nanoplasmid and one smaller band (Figure S2). In the second gel shift assay, only one correct size band was still observed for Cas9-CLIPT Nanoplasmid. After multiple freeze/thaws, the Control Nanoplasmid becomes a heterogeneous template, while the Cas9-CLIPT Nanoplasmid remains a homogeneous template.

To examine whether Cas9-CLIPT could be used to engineer a therapeutically relevant CAR T cell, we electroporated T cells with Nanoplasmid templates and an sgRNA targeted to the *TRAC* locus complexed within an *Sp*Cas9 RNP. In short, we metabolically primed[41,42] our T cells with a 3-day activation in TexMACS media, electroporated on day 3 using a Lonza 4D-Nucleofector X Unit system, recovered the T cells in ImmunoCult-XF with interleukin-7 (IL-7)/IL-15 and small molecules, and then expanded the T cells for 7 days in ImmunoCult-XF with IL-7/IL-15 post-EP (Figure 1C). The use of either TexMACS or ImmunoCult-XF media alone did not significantly impact the knock-in rate (Figure S3). We used 2 μg Cas9-CLIPT and Control donor template per 1 million cells because this optimal donor DNA concentration preserved high knock-in while maintaining T cell viability and expansion (Figure S4). Thirty minutes post-EP, we recovered the cells with the DNA-PK inhibitor Nedisertib (M3814) to block NHEJ and promote HDR DNA repair (Figure S5). On day 5 post-EP (day 8), there was a 1.7-fold increase in CAR^+ cells when using Cas9-CLIPT as the donor template (Cas9-CLIPT: 61% [3%], Control: 36% [1%]; $p < 0.001$) versus Control *TRAC*-CAR T cells (data are reported as condition: mean [error]) (Figures 1D and 1E). Non-transfected cells are T cells that did not receive any treatment during manufacturing; they were cultured according to our manufacturing process. We produced Control *TRAC*-CAR T cells using a circular Control Nanoplasmid instead of linearizing the Control Nanoplasmid prior to EP, although the linear Control Nanoplasmid resulted in higher CAR knock-in efficiencies (Figure S6). We also tested PCR-generated tCTS dsDNA donor templates but found that Cas9-CLIPT Nanoplasmid had improved CAR knock-in efficiencies compared to the PCR-generated tCTS dsDNA donor template at all DNA doses (Figure S7).

The addition of PGA during RNP incubation and the addition of Nedisertib during post-EP T cell recovery further increased knock-in efficiencies.[25,37,43] We observed that greater than 98% of Cas9-CLIPT and Control *TRAC*-CAR T cells lacked expression of the endogenous TCR (Cas9-CLIPT: 99.5% [0.2%], Control: 99.2% [0.5%]) (Figure 1E). The percentages of CAR knock-in (Cas9-CLIPT: 62% [2%], Control: 37% [1%]) and TCR knockout (Cas9-CLIPT: 99.4% [0.3%], Control: 99.0% [0.6%]; $p < 0.001$) also remained unchanged until day 7 post-EP (Figure 1E). There were no significant differences between Cas9-CLIPT and Control *TRAC*-CAR T cell fold expansion (Cas9-CLIPT: 8.8 [3.5], Control: 10.0 [3.2], RNP only: 5.6 [1.0], No EP: 22 [6.5]) or viability (Cas9-CLIPT: 89.7% [3.8%], Control: 88.8% [5.6%], RNP only: 85.8% [3.3%], No EP: 93% [2.3%]) after manufacturing (Figure 1F). Though, both the EP of T cells and addition of donor template to Cas9-CLIPT and Control-*TRAC* CAR T cells hindered T cell fold expansion and viability in comparison to T cells electroporated with no donor template (RNP only) and T cells that were not electroporated but were incubated with Cas9-CLIPT Nanoplasmid (No EP) (Figure 1F).

Since the transport of Cas9-CLIPT into T cells could depend on the mechanics of the EP instrument, we adapted our workflow on two other EP devices: the Cellares (South San Francisco, CA) EP (CEP) system, an automated clinical-scale manufacturing system, and the Thermo Fisher Scientific Neon NxT system, a precursor to the large-scale Xenon EP device. The CEP system affords users fine control over key EP parameters and operates in batch mode to enable EP at clinical-scale. Though we use PGA during RNP incubation and Nedisertib during post-EP recovery in all in-house experiments, PGA and Nedisertib were not used during Cas9-CLIPT *TRAC*-CAR T cell manufacturing on the CEP system. In this system, a small-scale EP that uses 5 million T cells resulted in Cas9-CLIPT *TRAC*-CAR T cells with knock-in rates well above Control *TRAC*-CAR T cell conditions (CAR knock-in: Cas9-CLIPT: 26% [8%], Control: 5%; TCR knockout: Cas9-CLIPT: 88% [2%], Control: 90%) (Figure 1G). For a 50 million T cell EP using the CEP system (large-scale), CAR knock-in efficiency was 15% compared to 26% in small-scale CEP experiments (CAR knock-in: 15% [8%]; TCR knockout: 86% [2%]) (Figure 1G). Further optimization on the CEP system may enhance clinical-scale approaches. Cas9-CLIPT strategies also improved knock-in using the Thermo Fisher Scientific Neon NxT EP system at small-scale (Figure S8). A summary of different media, small molecules, and EP devices was collected (Table S1). These results demonstrate that the Cas9-CLIPT Nanoplasmid can increase knock-in efficiencies in various EP conditions on multiple EP instruments.

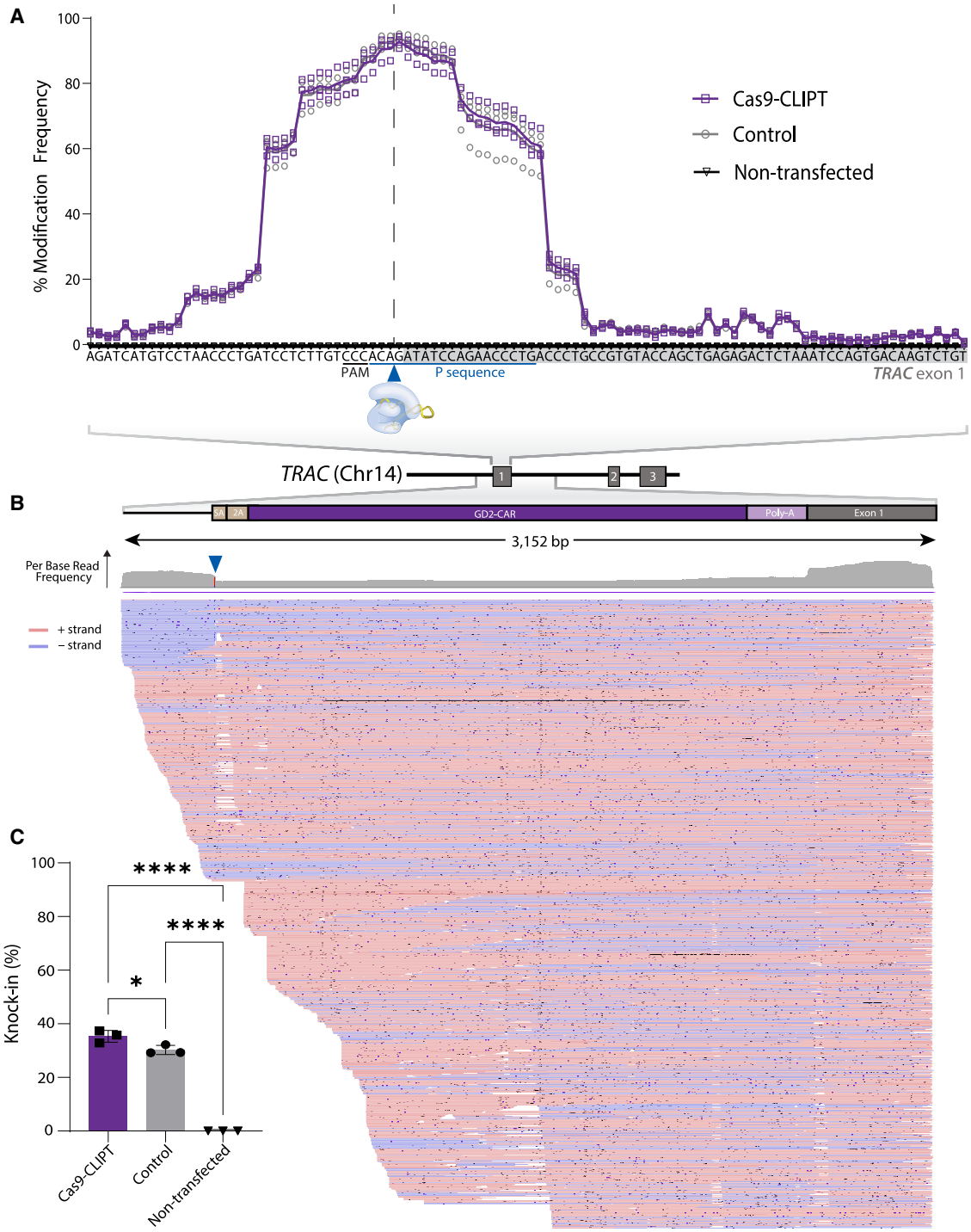

Figure 2. Long-read sequencing of on-target *TRAC* edits in Cas9-CLIPT CAR T cells

Genomic DNA was extracted on day 10 of manufacturing from Cas9-CLIPT CAR T cells, Control *TRAC*-CAR T cells, and non-transfected T cells. Regions surrounding the cut site were amplified via PCR, and amplicons were sequenced on the PromethION 24. (A) Indel editing efficiency in genomic DNA isolated from the CAR T products as measured by long-read sequencing. The modification frequency of each nucleotide around the *TRAC* cut site was calculated relative to the human genome *TRAC* reference sequence. The protospacer (P) and PAM are underlined, and a vertical dotted line indicates where Cas9 nuclease should create a dsDNA DSB. (B) Alignment of long-reads from sequencing the genomic DNA of Cas9-CLIPT CAR T cells from donor A to the expected transgene amplicon sequence (3,152 bp). Gray histogram indicates the relative

(legend continued on next page)

On-target genomic analysis of Cas9-CLIPT *TRAC*-CAR T cells

Insertion of the Cas9-CLIPT donor templates into the *TRAC* locus was confirmed by performing long-read sequencing[44] on genomic DNA isolated from the cell products. DNA was extracted on day 10 of manufacturing from Cas9-CLIPT and Control *TRAC*-CAR T cells from three different donors. The 3-kb regions of interest were amplified via PCR around the intended insertion site. Amplicons were sequenced using a long-read Oxford Nanopore Technologies instrument. The modification frequency of each base pair around the *TRAC* cut site relative to the wild-type sequence was calculated for Cas9-CLIPT and Control *TRAC*-CAR T cell amplicons by dividing by the number of reads not aligned to the wild-type sequences at each base pair with the total number of reads observed at each base pair. High on-target genome editing was observed, as indicated by high indel formation precisely at the *TRAC* target site (Figure 2A). There were no significant differences in the indel pattern between Cas9-CLIPT and Control *TRAC*-CAR T cells (Figure 2A). These alleles are predicted to result in a TCR knockout through frameshifts in the coding sequence and nonsense-mediated decay of the resulting *TRAC* mRNA transcripts. Notably, the alleles with full-length CAR insertion were robustly observed in the reads from sequencing (Figure 2B). An exact match to the GD2-CAR sequence throughout the transgene and at the junctions of the homology arms was observed (Figure 2B). These results are consistent with HDR-mediated precise knock-in of the desired CAR transgene sequences and NHEJ inhibition due to the use of Nedisertib during manufacturing. We estimated the allelic knock-in efficiency by dividing the number of reads aligned to the insert by the total number of reads aligned to both the edited and the unedited samples and found a higher percentage of precise insertions with Cas9-CLIPT (Cas9-CLIPT: 35% [2.2%], Control: 30% [1.7%], Non-transfected: 0.0% [0.0%]; $p = 0.038$) (Figure 2C).

While we estimated the allelic knock-in efficiency by dividing the number of reads aligned to the insert by the total number of reads aligned to both the edited and the unedited samples and found a higher percentage of precise insertions with Cas9-CLIPT (Figure 2C), the allelic knock-in efficiencies are lower than the observed flow cytometry results (Figure 1E). This is likely due to PCR bias.[45] Since our CAR T cell products are not 100% efficient, there are still edited and unedited T cells within one sample. When performing PCR on one sample, the DNA from unedited cells will produce a shorter PCR product than the DNA from edited cells due to the size of the transgene insert. Due to PCR bias favoring smaller amplicons during annealing and extension steps, it is easier for the smaller, unedited DNA fragments to be amplified during PCR than the larger, edited DNA fragments.[45] Thus, it is likely the allelic knock-in efficiencies are not as high as the flow cytometry knock-in efficiencies because it was easier to amplify the unedited DNA than the edited DNA.

Off-target genomic analysis of Cas9-CLIPT *TRAC*-CAR T cells

Though CRISPR-Cas9 is a precise genome editing tool, it is possible that the sgRNA used to edit the *TRAC* locus of T cells could bind elsewhere in the human genome, causing unintended off-target edits.[46] To determine whether any off-target sites exist in Cas9-CLIPT *TRAC*-CAR T cells, we performed whole genome sequencing (WGS) (Figure 3A). WGS allows for unbiased tracking of integration sites of our transgene since WGS does not have PCR amplification biases nor does it require the nomination of off-target sites. Genomic DNA was prepared for long-read nanopore sequencing via Oxford Nanopore Technologies and aligned to a reference sequence containing the CAR transgene. Successful mapping to the reference human genome provided 30X coverage of the genome. On-target integration was observed in 3,270 of 3,367 reads (97.3%) with alignment to the CAR transgene (Figure 3B). Off-target integration was minimally observed in all but two human chromosomes (Figure 3B). Some of the off-target hits are likely hits because the single-chain variable fragment (scFv) of the CAR transgene aligns with the immunoglobulin loci found in chromosomes 2 and 22.[47] Off-target integration sites were identified from reads that aligned to both the transgene and the human genome if there was a minimum alignment length of 150 bp and a minimum MAPQ value of 30 (Figure 3C). Overall, the few number of reads aligned at off-target sites is likely not cause for concern for off-target integration when using Cas9-CLIPT Nanoplasmid.

Phenotypic analysis of Cas9-CLIPT *TRAC*-CAR T cells

Ex vivo culture of CAR T cells with artificial activation and high concentrations of cytokines can trigger differentiation into short-lived effector T cells that struggle to persist *in vivo*.[17,48] In contrast, preserving the naive, stem cell memory T cell population during CAR T cell manufacturing can increase CAR T cell persistence. Control *TRAC*-CAR T cells undergoing "metabolic priming," or switching media formulation post-EP, have improved stem cell memory properties.[41,42] We analyzed whether Cas9-CLIPT *TRAC*-CAR T cells cultured in a similar manner to metabolically primed CAR T cells would have a similar phenotype. Spectral flow cytometry was used to distinguish the CAR^+/TCR^- population of Cas9-CLIPT *TRAC*-CAR T cells and profile the surface markers for CD8, CD4, and stem cell memory (Figure S9), such as CD45RA, CCR7, and CD62L. These stem cell memory markers decrease as T cells differentiate into effector cells (Figure 4A). We found that 59% [11%] of our Cas9-CLIPT *TRAC*-CAR were positive for cytotoxic CD8 (Figure S10), indicating a balanced CD8 and CD4 T cell product. In addition, T cells can be classified as naive (T_N) ($CD45RA^+/CD62L^+/CCR7^+$), naive-central memory ($T_{N\text{-}CM}$) ($CD45RA^+/CD62L^+/CCR7^-$), central memory (T_{CM}) ($CD45RA^-/CD62L^+/CCR7^+$), central-effector memory ($T_{CM\text{-}EM}$) ($CD45RA^-/CD62L^+/CCR7^-$),

number of reads at each base pair aligned to the insert and homology arms. Red indicates the negative strand; blue indicates the positive strand. (C) Allelic knock-in efficiency as measured by long-read sequencing. Knock-in efficiency is defined as the number of reads aligned to the transgene divided by the total number of reads aligned to both the transgene and the reference genome. DSB, double-stranded break. Three donors, $N_{Cas9\text{-}CLIPT} = N_{Control} = N_{Non\text{-}transfected} = 6$. Error bars represent mean and standard deviation. Statistical significance was calculated with paired t-tests; $^*p < 0.05$; $^{****}p < 0.0001$.

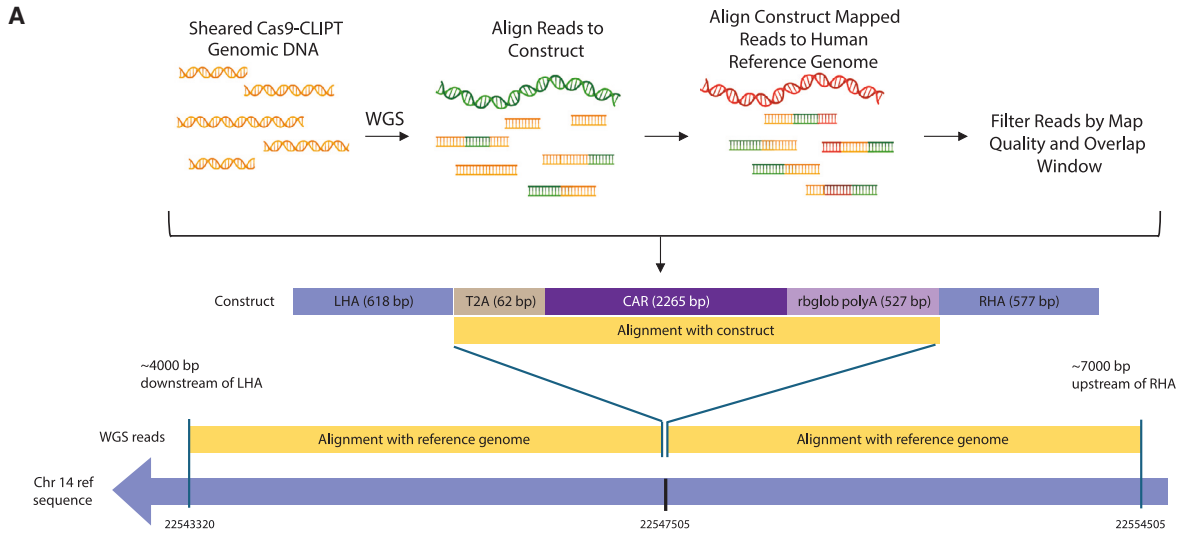

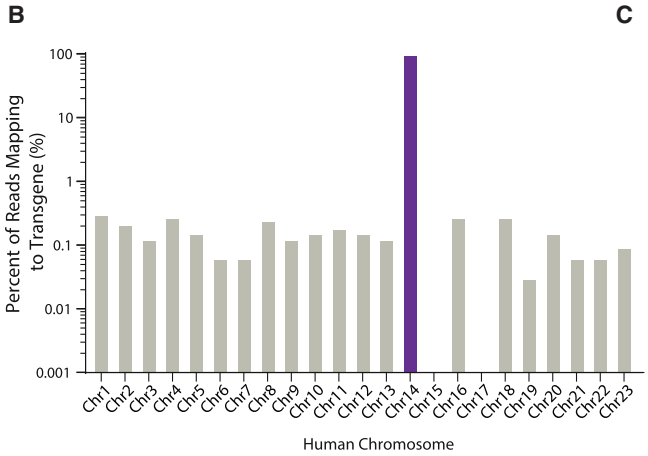

C

Integration Site	Number of Supporting Reads	Average 14g2a Alignment Length (Gaps Included)	Average MAPQ	Average Chromosomal Alignment Length (Gaps Included)	Average MAPQ
Chr 14 (on target)	3270	796.4	59.9	580.0	59.9
Chr 1	10	800.2	60	5612.6	60
Chr 2	2	824.1	60	7131.6	60
Chr 3	4	717.3	60	4128.5	60
Chr 4	9	906.8	60	4960.8	60
Chr 5	5	795.8	60	5443.6	60
Chr 6	2	603.0	60	14319.0	60
Chr 7	2	903.0	60	4019.0	60
Chr 8	8	771.1	60	4757.8	60
Chr 9	4	847.0	60	6021.3	60
Chr 10	5	780.2	60	4734.8	59
Chr 11	6	797.0	60	3262.2	60
Chr 12	5	788.8	60	7013.2	60
Chr 13	4	727.0	60	8351.3	60
Chr 15	0	N/A	N/A	N/A	N/A
Chr 16	9	746.3	60	4009.7	60
Chr 17	0	N/A	N/A	N/A	N/A
Chr 18	9	796.9	60	5874.4	57
Chr 19	1	261	60	4754	60
Chr 20	5	757.0	60	6312.0	60
Chr 21	2	548.0	60	1688.0	60
Chr 22	2	905.5	60	5283.0	60
Chr 23	3	376.5	60	5120.3	53

Figure 3. Whole-genome sequencing of Cas9-CLIPT *TRAC*-CAR T cells indicates minimal off-target effects

Genomic DNA was extracted from Cas9-CLIPT *TRAC*-CAR T cells and sequenced via Oxford Nanopore Technologies Sequencing for unbiased whole-genome sequencing (WGS) to determine off-target sites. (A) Schematic of unbiased WGS alignment. Sequencing reads were aligned to the transgene, and hits were then mapped to the human genome. After filtering with an overlap window threshold, reads that aligned to both the transgene and human genome were considered an off-target integration site. (B) Percentage of reads that were considered an off-target integration site on each chromosome on a log scale. Chromosome 14 contains the on-target *TRAC* locus for Cas9-CLIPT *TRAC*-CAR T cells. (C) The number of integration site reads on each chromosome, and the corresponding average alignment length of the read to the transgene (14g2a) and human genome (chromosomal). The average MAPQ of each alignment is also reported. One donor, $N_{Cas9\text{-}CLIPT} = 1$.

effector memory (T_{EM}) ($CD45RA^-/CD62L^-/CCR7^-$), or terminal effector (T_{EMRA}) ($CD45RA^+/CD62L^-/CCR7^-$). We observed that Cas9-CLIPT *TRAC*-CAR T cells were 8% [6%] T_N, 37% [10%] $T_{N\text{-}CM}$, 9% [5%] T_{CM}, 30% [15%] $T_{CM\text{-}EM}$, 7% [3%] T_{EM}, and 7% [3%] T_{EMRA}, respectively, across three biological donors, indicating a large portion of naive T cells in the pre-infusion product (p ($T_{N\text{-}CM}$ vs. T_N, T_{CM}, T_{EM}, or T_{EMRA}) = 0.010, 0.013, 0.008, or 0.0083) (Figures 4B and 4C).

Potency of Cas9-CLIPT *TRAC*-CAR T cells

We evaluated the potency of Cas9-CLIPT *TRAC*-CAR T cells against the $GD2^+$ neuroblastoma cell line, CHLA-20, by measuring cytotoxicity after co-culture. We seeded CHLA-20 target cells in 96-well plates and cultured them for 24 h, after which Cas9-CLIPT and Control *TRAC*-CAR T cells were added at 10:1, 5:1, 2.5:1, and 1.25:1 effector:target (E:T) ratios (Figure 4D). All groups successfully lysed CHLA-20 cells over 72 h at each E:T ratio (Figures 4E and S11) with no differences in the extent of cytotoxicity for a 1.25:1 E:T after 72 h of co-culture (Cas9-CLIPT: 66% [22%], Control: 70% [19%], Cancer only: 0% [0%]; p (Cas9-CLIPT or control vs. cancer only) = 0.001) (Figure 4F). These results demonstrate that our Cas9-CLIPT integration strategy can create potent *TRAC*-CAR T cells *in vitro*.

Large transgene knock-in using Cas9-CLIPT

The immune response of T cells to foreign intracellular circular plasmid dsDNA limits the knock-in of large (>2 kb) transgenes.[23]

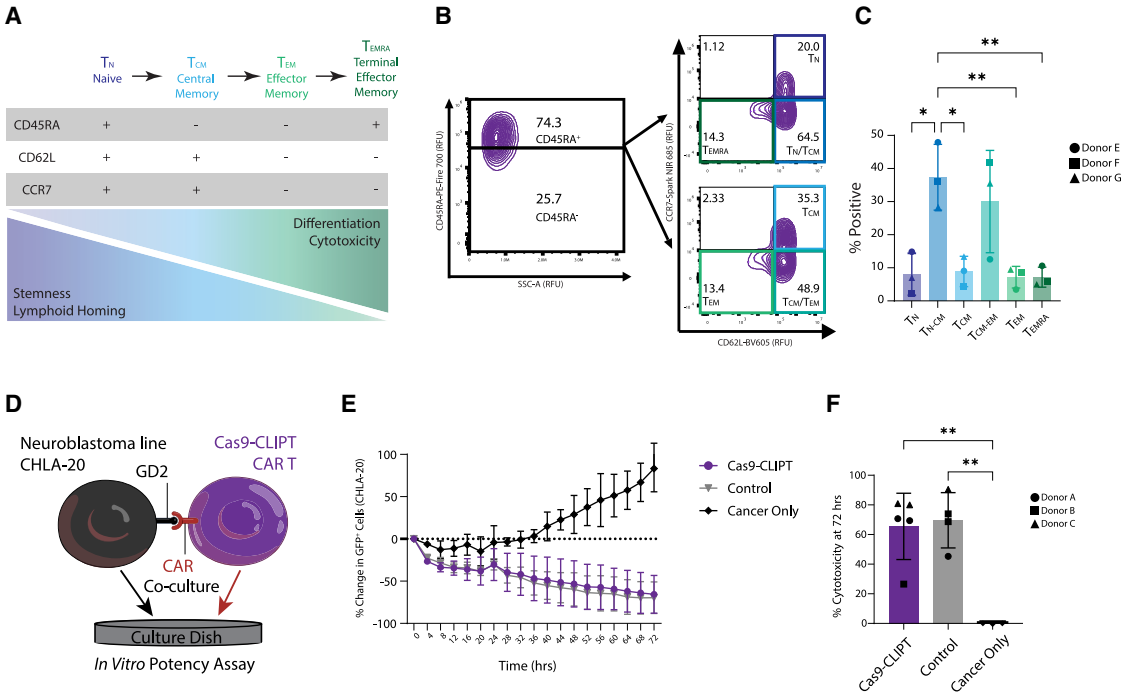

Figure 4. Cas9-CLIPT *TRAC*-CAR T cells are stem cell memory-like and potent against solid tumor cells *in vitro*

(A) Cas9-CLIPT *TRAC*-CAR T cells were analyzed for expression of stem cell memory T cell surface markers by spectral flow cytometry on day 7 post-EP. (B) Representative contour plots of CD62L vs. CCR7 expression in CD45RA ± populations of Cas9-CLIPT *TRAC*-CAR T cells. (C) Percentage of naive ($CD45RA^+/CD62L^+/CCR7^+$), naive-central memory ($CD45RA^+/CD62L^+/CCR7^-$), central memory ($CD45RA^-/CD62L^+/CCR7^+$), central-effector memory ($CD45RA^-/CD62L^+/CCR7^-$), effector memory ($CD45RA^-/CD62L^-/CCR7^-$), and terminal effector ($CD45RA^+/CD62L^-/CCR7^-$) T cells. (D) $GD2^+$ neuroblastoma CHLA-20 cells were plated in 96-well plates 24 h before *TRAC*-CAR T cell addition. The potency was measured continuously for up to 72 h. (E) Percent change in GFP fluorescence from $GD2^+$ CHLA-20 neuroblastoma cells vs. time in cancer/Cas9-CLIPT or Control *TRAC*-CAR T cell co-cultures for a 1.25:1 E:T ratio. (F) Percent cytotoxicity at 72 h for cancer/Cas9-CLIPT and Control *TRAC*-CAR T cells at an E:T ratio of 1.25:1 compared to a cancer only control. GFP, green fluorescent protein; E:T, effector:target ratio. Three donors, $N_{Cas9\text{-}CLIPT} = N_{Control} = 6$. Error bars represent mean and standard deviation. Statistical significance was determined with one-way ANOVA; $^*p < 0.05$; $^{**}p < 0.01$.

To explore whether Cas9-CLIPT strategies could be adapted to larger transgenes, we constructed a circular Cas9-CLIPT nuclear factor of activated T cells-mCherry (NFAT-mCh) Nanoplasmid. In addition to containing an anti-GD2 CAR within the donor template, the transgene insert sequence contains an NFAT response element with minimal IL-2 promoter[49,50] to drive expression of a downstream fluorescent mCherry reporter protein (Figure 5A). NFAT is a key transcription factor that initiates transcription of IL-2 during T cell activation through signaling from the endogenous TCR or an integrated CAR.[51] The same CAR T cell manufacturing process used to produce Cas9-CLIPT *TRAC*-CAR T cells was used to produce NFAT-mCh *TRAC*-CAR T cells. Using the large NFAT-mCh Nanoplasmid, we observed high knock-in efficiency via flow cytometry assays (NFAT-mCh knock-in: 38% [4%]) and minimal TCR expression (NFAT-mCh TCR knockout: 99% [0.5%]) (Figure 5B), indicating that our Cas9-CLIPT strategy can successfully edit T cells with >5 kb gene insertions. RNP incubation with PGA prior to the addition of NFAT-mCh Nanoplasmid significantly increased CAR knock-in and TCR knockout efficiencies and is necessary for clinically relevant efficiencies of NFAT-mCh *TRAC*-CAR T cells (Figure S8).

To demonstrate whether our integrated construct resulted in functional CAR T cells, we stimulated NFAT-mCh and Cas9-CLIPT *TRAC*-CAR T cells with either phorbol 12-myristate 13-acetate (PMA)/ionomycin or the $GD2^+$ neuroblastoma cell line, CHLA-20. We performed flow cytometry after 24 h to measure the NFAT-driven expression of mCherry in CAR^+ T cells. Stimulation of T cells with either method successfully induced expression of mCherry to different extents in CAR^+ NFAT-mCh T cells, which we gated into 'high' and 'low' fractions (mCh high and mCh low) in the CAR^+/mCh^+ population (Figure 5C). The low gate includes some mCherry expression driven by NFAT in the absence of stimulation, while the high gate is specific to antigen or PMA/ionomycin stimulation. Stimulated NFAT-mCh CAR T cells had significantly higher percentages of mCh High cells than unstimulated NFAT-mCh or Cas9-CLIPT CAR T cells (NFAT-mCh + PMA/ionomycin: 32.1% [2.7%], NFAT-mCh + CHLA-20: 7.2% [1.4%], NFAT-mCh: 1.6% [0.4%], Cas9-CLIPT: 0.01% [0.02%]; p [NFAT-mCh + PMA-ionomycin or CHLA-20 vs. NFAT-mCh or Cas9-CLIPT] < 0.001; p (NFAT-mCh + PMA/ionomycin vs. CHLA-20) < 0.0001) (Figure 5D). Unstimulated NFAT-mCh CAR T cells also had higher

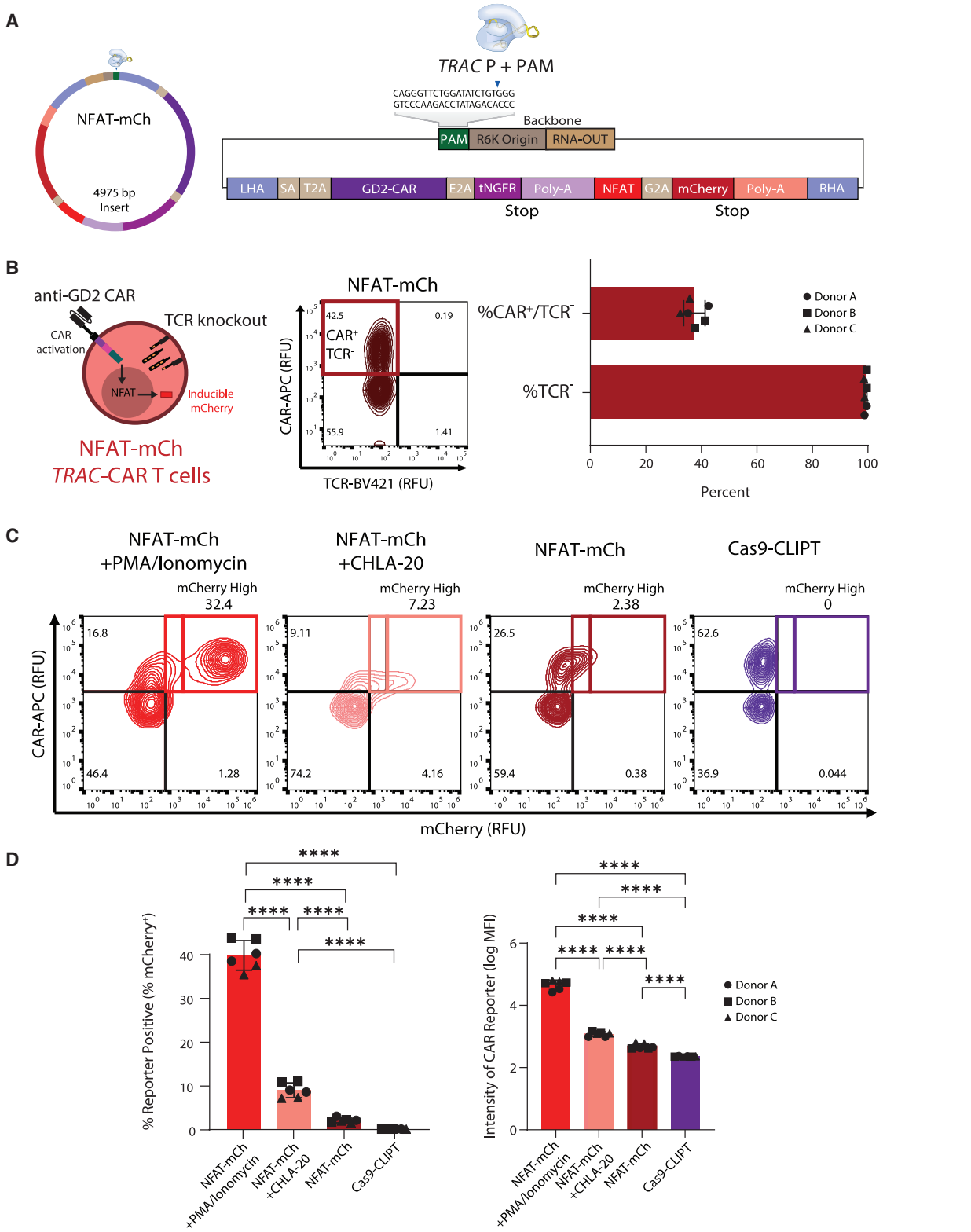

(legend on next page)

expression of mCh Low cells than those stimulated with PMA/ionomycin or CHLA-20 cells, indicating a low-level activation of NFAT (NFAT-mCh + PMA/ionomycin: 2.0% [0.5%], NFAT-mCh + CHLA-20: 5.6% [0.4%], NFAT-mCh: 11.7% [2.7%], Cas9-CLIPT: 0.5% [0.07%]; p (NFAT-mCh vs. NFAT-mCh + PMA/ionomycin or CHLA-20 or Cas9-CLIPT) < 0.001; p (NFAT-mCh + CHLA-20 vs. NFAT-mCh + PMA/ionomycin or Cas9-CLIPT) < 0.001 or = 0.002) (Figure S12). Antigen-stimulated NFAT-mCh CAR T cells had higher mCherry mean fluorescence intensity (MFI) than unstimulated cells, showing higher mCherry expression within the CAR$^+$ population (NFAT-mCh + PMA/ionomycin: 4.7 [0.2], NFAT-mCh + CHLA-20: 3.1 [0.1], NFAT-mCh: 2.7 [0.1], Cas9-CLIPT: 2.4 [0.01]; p (NFAT-mCh + PMA/ionomycin vs. NFAT-mCh + CHLA-20 or NFAT-mCh or Cas9-CLIPT) < 0.001; p (NFAT-mCh + CHLA-20 vs. NFAT-mCh or Cas9-CLIPT) < 0.001; p (NFAT-mCh vs. Cas9-CLIPT) < 0.001) (Figure 5D). Stimulation by GD2 antigens by the CHLA-20 neuroblastoma resulted in weaker mCherry expression versus PMA/ionomycin stimulation, as the former had a higher percentage of mCh Low cells and correspondingly a lower percentage of mCh High cells (Figures 5C and S12).

On-target genomic analysis of NFAT-mCh *TRAC*-CAR T cells

Similar to the Cas9-CLIPT *TRAC*-CAR T cells, we also confirmed precise insertion via HDR of the NFAT-mCh transgene at the genomic level via long-read sequencing[44] on genomic DNA isolated from the NFAT-mCh *TRAC*-CAR T cell products. DNA was extracted on day 10 of manufacturing from NFAT-mCh *TRAC*-CAR T cells from three different donors. The regions of interest were amplified via PCR around the intended insertion site. Amplicons were sequenced using a long-read Oxford Nanopore Technologies instrument. The modification frequency of each base pair around the *TRAC* cut site relative to the wild-type sequence was calculated for NFAT-mCh *TRAC*-CAR T cell amplicons by dividing by the number of reads not aligned to the wild-type sequences at each base pair with the total number of reads observed at each base pair. High on-target genome editing was observed, as indicated by high indel formation precisely at the *TRAC* target site (Figure 6A). There were no significant differences in the indel pattern between NFAT-mCh, Cas9-CLIPT, and Control *TRAC*-CAR T cells (Figure 6A). We estimated the allelic knock-in efficiency by dividing the number of reads aligned to the insert by the total number of reads aligned to both the edited and the unedited samples and found precise insertions of NFAT-mCh (NFAT-mCh: 14% [2.4%]; p < 0.0001) (Figure 6B).

Potency of NFAT-mCh *TRAC*-CAR T cells

Despite the lower expression, we detected NFAT-driven mCherry fluorescence in images of Cas9-CLIPT NFAT-mCh CAR T cells with GD2$^+$ neuroblastoma cells on the IncuCyte live-imaging platform (Figure 6C). mCherry fluorescence was detected for up to 72 h (Figure S13), indicating sustained expression with antigen exposure. The number of mCh$^+$ cells decreased with lower E:T ratios (NFAT-mCh: (10:1) 556 [228], (5:1) 459 [190], (2.5:1) 235 [98], (1.25:1) 141 [49], Cas9-CLIPT: (10:1) 5 [3], (5:1) 2 [1], (2.5:1) 2 [1], (1.25:1) 3 [2]; p (10:1, 5:1, 2.5:1, 1.25:1) = 0.0004) (Figure S13), while the average intensity was unchanged at 12 h (NFAT-mCh: (10:1) 30 [1], (5:1) 29 [5], (2.5:1) 25 [2], (1.25:1) 25 [2]) (Figure S14). At 10:1, 5:1, 2.5:1, and 1.25:1 E:T ratios, all groups successfully lysed CHLA-20 cells over 72 h at each E:T ratio (Figure 6D) with no differences in the extent of cytotoxicity for a 1.25:1 E:T after 72 h of co-culture (NFAT-mCh: 64% [14%], cancer only 0% [0%]; p [NFAT-mCh vs. cancer only] = 0.005) (Figure 6E). These results indicate that our Cas9-CLIPT integration strategy can create potent GD2 *TRAC*-CAR T cells via a functional large transgene.

DISCUSSION

We have demonstrated a streamlined manufacturing process of virus-free *TRAC*-CAR T cells[17,41] by simplifying the preparation of donor templates and increasing knock-in of small and large transgenes into T cells. By adding a single *TRAC* target sequence into a CAR-containing Nanoplasmid, we made Cas9-CLIPT, eliminating the costly, time-consuming, and challenging production of linearized HDR donor templates via PCR or restriction digestion of circular plasmids. Nanoplasmid DNA can be easily manufactured within recombinant bacteria at scale using GMP conditions[29,33] and is already in use in clinical trials,[30] making the Cas9-CLIPT platform adaptable for clinical production of *TRAC*-CAR T cell therapies. Manufacturing *TRAC*-CAR T cells with Cas9-CLIPT significantly increases knock-in efficiencies to mirror efficiencies commonly observed when using retroviruses to produce CAR T cells.[39]

CAR knock-in was assisted in some cases by including PGA during RNP complexing, as the knock-in efficiency decreases without it (Figure S8). PGA is an anionic polymer that is theorized[26] to prevent RNP aggregation. However, the addition of PGA to other non-viral CAR T cell workflows has had inconsistent effects, with some studies observing seemingly no benefit to knock-in or viability.[23] It is possible that the addition of PGA to non-viral CAR T cell manufacturing is donor dependent. However, successful EP is dependent on the charge

Figure 5. Large knock-in using Cas9-CLIPT enables fluorescent reporter of CAR activation

(A) Schematic of Cas9-CLIPT NFAT-mCh DNA containing a GD2 CAR transgene under the control of the endogenous *TRAC* promoter and an mCherry reporter gene conditionally expressed with NFAT binding domains and the minimal IL-2 promoter targeted to the *TRAC* locus. Cas9-CLIPT templates contain a *TRAC* gRNA site with PAM to be linearized by the RNP. (B) NFAT-mCh CAR T cells contain an inducible mCherry reporter gene dependent on CAR activation. A representative contour plot and bar graph depict NFAT-mCh CAR T cell TCR and CAR expression. (C) One million NFAT-mCh CAR T cells were stimulated with either PMA/ionomycin or 200,000 CHLA-20 neuroblastoma cells for 24 h. Stimulated and unstimulated Cas9-CLIPT NFAT-mCh or Cas9-CLIPT *TRAC*-CAR T cell samples were then assayed for NFAT-driven mCh expression. Representative contour plots detail CAR vs. mCh expression. (D) Bar graphs of percentage of CAR$^+$/mCh High populations and mCh MFI. MFI, mean fluorescence intensity. Three donors, $N_{Cas9\text{-}CLIPT} = N_{NFAT\text{-}mCh} = 6$. Error bars represent mean and standard deviation. Statistical significance was determined with one-way ANOVA; ****p < 0.0001.

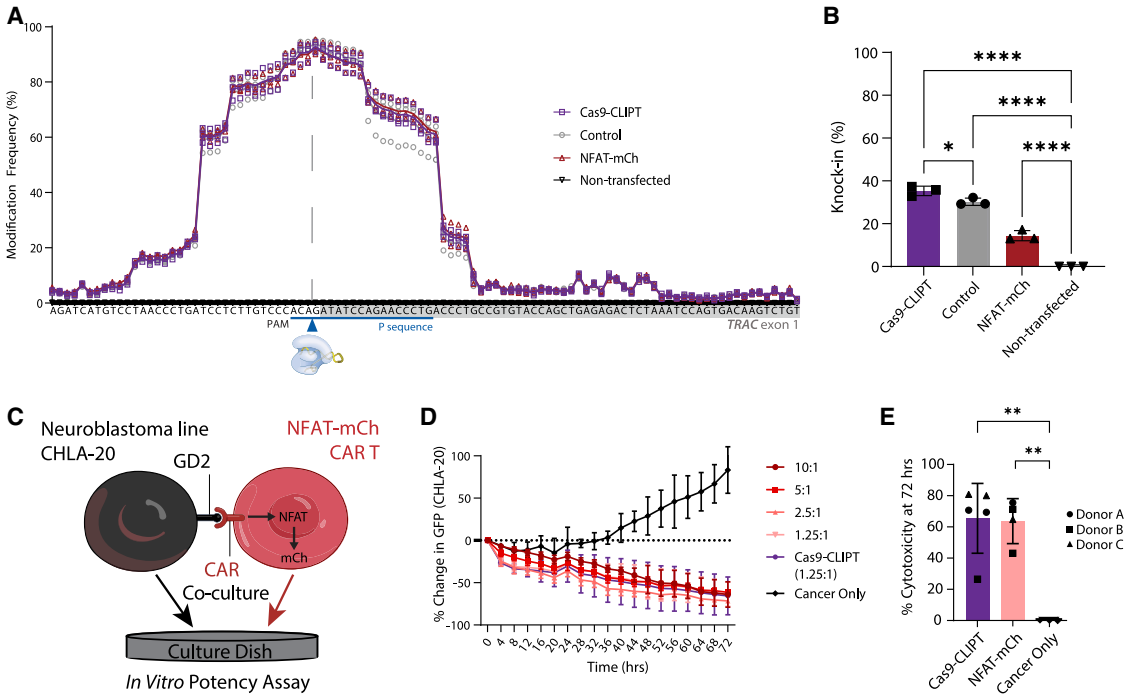

Figure 6. Long-read sequencing of on-target *TRAC* edits in potent NFAT-mCh CAR T cells

Genomic DNA was extracted on day 10 of manufacturing from Cas9-CLIPT, NFAT-mCh, and Control *TRAC*-CAR T cells, as well as non-transfected T cells. Regions surrounding the cut site were amplified via PCR, and amplicons were sequenced on the PromethION 24. (A) Indel editing efficiency in genomic DNA isolated from the CAR T products as measured by long-read sequencing. The modification frequency of each nucleotide around the *TRAC* cut site was calculated relative to the human genome *TRAC* reference sequence. The protospacer (P) and PAM are underlined, and a vertical dotted line indicates where Cas9 nuclease should create a dsDNA DSB. (B) Allelic knock-in efficiency as measured by long-read sequencing. Knock-in efficiency is defined as the number of reads aligned to the transgene divided by the total number of reads aligned to both the transgene and the reference genome. (C) GD2$^+$ neuroblastoma GFP$^+$ CHLA-20 cells were plated in 96-well plates 24 h before *TRAC*-CAR T cell addition. GFP expression was measured continuously for up to 72 h. (D) Percent change in GFP fluorescence from GD2$^+$ CHLA-20 neuroblastoma cells vs. time in cancer/NFAT-mCh CAR T cell co-cultures for E:T ratios of 10:1, 5:1, 2.5:1, or 1.25:1 and (E) bar graph of extent of cytotoxicity at 72 h for 1.25:1 E:T ratios. Error bars represent mean and standard deviation. Three donors, $N_{Cas9\text{-}CLIPT\ NFAT\text{-}mCh} = 6$. Error bars represent mean and standard deviation. Statistical significance was determined with paired t-tests; $^*p < 0.05$; $^{**}p < 0.01$; $^{****}p < 0.0001$.

of its cargo,[52,53] so neutralization of positive Cas9 charges by negatively-charged PGA may prevent inhibitory interactions with the heterogeneous surface charge of T cells,[54] thereby eliminating a potential barrier to delivery. While we employed PGA, it did not affect the extent of Cas9-CLIPT Nanoplasmid linearization, which manifests as a heavier band than linearized Control Nanoplasmid in our gel electrophoresis assay (Figure 1B).

Cas9-CLIPT bound to *Sp*Cas9 with NLS may increase trafficking to the nucleus to increase knock-in, similar to ssDNA HDR donor templates bound with Cas9 via truncated target sequences.[25] Bound Cas9 may also cleave the donor template and genomic target efficiently, leading to an increased chance of HDR due to the proximity of homologous sequences to the on-target site.[34,55] Other non-viral processes have incorporated gRNA cut sites to increase the knock-in of a CD19 CAR[22] and a reporter gene.[37] The latter study also integrated a large (6.3 kb) multicistronic CAR transgene,[37] which bypasses the usual 1.5-kb limit for linearized HDR donor templates in T cells.[18,26] We also bypass this limit by achieving high knock-in with our 5.0-kb inducible NFAT-mCh GD2-CAR construct with a single gRNA cut site as opposed to the double cut variant. Finally, homology-independent targeted integration (HITI) templates with a single cleavage site perform differently from HITI templates with two cleavage sites for non-HDR knock-in within mice *in vivo*.[56] Mechanisms within mammalian cells that distinguish one vs. two cleaved ends of the template may not involve bound Cas9, as with our Cas9-CLIPT strategy, but still promote transgene knock-in for our human T cell system.

Other end joining integration processes like microhomology-mediated end joining (MMEJ) or HMEJ are also repair mechanism possibilities when using an sgRNA target site.[34,35,55] MMEJ is an end joining repair mechanism that uses short homology arms (5–25 bp long) to integrate transgenes.[34] However, MMEJ can introduce many indels at homology arm junctions as well as random integration directions.[34] HMEJ is also an end joining repair mechanism that uses long homology arms (~800 bp long) to integrate transgenes.[34] It is possible that Cas9-CLIPT could integrate the entire linearized

Nanoplasmid, including the plasmid backbone located downstream of the right homology arm. However, in our Cas9-CLIPT design, poly-adenylation sequences at the end of the CAR transgene and the presence of the right homology arm likely prevent the Nanoplasmid backbone from being transcribed via the endogenous *TRAC* promoter or even integrated in our proliferating cells. We observed all Cas9-CLIPT *TRAC*-CAR T cell sequencing reads in Integrative Genomics Viewer (IGV). According to the sequences at the junctions where the left and right homology arms meet the transgene, indels and random direction integrations were not observed and therefore we have concluded that MMEJ repairs were not observed. All reads that contained transgene sequences were continuous and showed no gaps in sequences at the homology arms, indicating that HDR was likely the DNA repair mechanism used when generating Cas9-CLIPT *TRAC*-CAR T cells. This may be due to Nedisertib addition, known to block end joining repair mechanisms (Figure S5).[25,43] Non-HDR integration events can also be reduced while increasing HDR insertion by simultaneously inhibiting DNA-PK and polymerase theta-mediated end joining with small molecule inhibitors Nedisertib, ART558,[38] and AZD7648.[57] Control *TRAC*-CAR T cell knock-in efficiencies tripled when treated with Nedisertib and ART558 compared to untreated control TRAC-CAR T cells (Figure S5), indicating these drugs could be used to further increase knock-in efficiency with the Cas9-CLIPT strategy in future studies.[57] Treatment with both Nedisertib and ART558 significantly decreased *TRAC*-CAR T cell count compared to untreated *TRAC*-CAR T cells and *TRAC*-CAR T cells treated with only Nedisertib. Therefore, the combination of DNA-PK inhibitors and polymerase theta-mediated end joining inhibitors would need to be optimized in the future to ensure clinically relevant CAR T cell yields.

Knock-in of Cas9-CLIPT Nanoplasmid on the CEP system provides a proof-of-principle and indicates the feasibility of moving to automated and scaled-up *TRAC*-CAR T cell therapy biomanufacturing (Figure 1G). This move is likely to have significant benefits compared to the current commercial CAR T cell manufacturing workflow, as the ability of Cellares Cell Shuttle technology to manufacture 16 cell therapy batches in parallel reduces facility size and labor requirements. Furthermore, efficiency and performance gains rooted in the Cell Shuttle's automated handling systems and closed ISO8 internal environment could significantly decrease process failure rates and reduce batch prices. The cells can be processed in a fully closed, single-use cartridge. The integrated Cellares platform using the Cas9-CLIPT strategy is estimated to produce 10 times more cell therapy batches per year, with the same footprint and the same workforce, as in conventional contract development and manufacturing organizations. At such a scale, the CEP system has the potential to produce relevant doses of *TRAC*-CAR T cells for future *in vivo* experiments. Successful *in vivo* experiments have been performed with the transgene sequence of the Control construct.[17,41] The *in vivo* results in these published studies demonstrate solid tumor regression with the same third-generation CAR, transgene, and CRISPR editing strategy from a linear dsDNA template. Since the memory phenotype of our Cas9-CLIPT *TRAC*-CAR T cells matches the phenotypes observed in our Control *TRAC*-CAR T cells and the CAR T cells produced in published studies,[17,41] we anticipate that our Cas9-CLIPT *TRAC*-CAR T cells will have similar functional properties regarding potency and persistence *in vivo* (Figure 4B).

Our Cas9-CLIPT donor template simplifies non-viral CAR T cell production by eliminating expensive, difficult-to-scale-up dsDNA linearization and purification steps. We demonstrate an 8.8-fold expansion of Cas9-CLIPT *TRAC*-CAR T cells during manufacturing while increasing CAR knock-in efficiency to over 60% with a 2.2-kb insert. Compared to recombinant adeno-associated virus (rAAV) donor templates, we could effectively insert an inducible fluorescent reporter (5.5 kb transgene) at rates exceeding 35%, bypassing the cargo limit of 4.5 kb for rAAV.[58,59] Cas9-CLIPT likely has the potential to knock-in even larger transgenes, enabling the inclusion of the co-expression of additional genes. The overexpression of transcription factors like PRODH2[60] or FOXO1[61,62] could increase metabolic fitness or memory formation in *TRAC*-CAR T cells. Armored CAR T cells have also been engineered to express SynNotch receptors, which more reliably express downstream cytokines, like IL-2, at higher rates than NFAT response elements[63] and logic gates to CAR expression to mitigate off-target cytotoxicity.[64] The integration of these multifunctional designs using Cas9-CLIPT at clinical scale could ultimately further improve the safety and efficacy of gene-edited immune cell therapies.

MATERIALS AND METHODS

Cell lines

$GD2^+$ human neuroblastoma CHLA-20 cells were gifted to us by Dr. Mario Otto (University of Wisconsin-Madison). These cells were cultured in Dulbecco's Modified Eagle's Medium (DMEM) supplemented with 10% fetal bovine serum (FBS) (Gibco, Thermo Fisher Scientific, Waltham, MA) and 1% penicillin/streptomycin (P/S) (Gibco, Thermo Fisher Scientific). AkaLUC-GFP CHLA-20 cells were created through viral transduction by Dr. James Thomson (Morgridge Institute for Research). In short, Phoenix cells (American Type Culture Collection [ATCC], Manassas, VA) were grown in DMEM with 10% FBS and 1% P/S and selected with 1 μg/mL diphtheria toxin (Cayman Biologics, Ann Arbor, MI) and 300 μg/mL hygromycin (Thermo Fisher Scientific). The selection of transgene-positive cells was confirmed by flow cytometry for mouse Lyt2 expression as a reporter gene (BioLegend, San Diego, CA). We grew 3T3 cells in DMEM with 10% FBS and 1% P/S. Cell authentication was performed using short tandem repeat analysis (Idexx BioAnalytics, Westbrook, ME) and per ATCC guidelines using cell morphology, growth curves, and *Mycoplasma* testing within 6 months using the MycoStrip Mycoplasma Detection Kit (Invitrogen, Waltham, MA). Cell lines were maintained in culture at 37°C in 5% CO_2.

Nanoplasmid constructs

A GD2-CAR plasmid construct encoding a 2A.14G2A-CD28-OX40-CD3ζ CAR gifted to us by Malcolm Brenner (Baylor College of Medicine) was synthesized and the sequence verified (Control) (GenScript, Piscataway, NJ). An additional sequence encoding the *TRAC* sgRNA plus PAM (5′-CAGGGTTCTGGATATCTGTGGG-3′) was cloned

into the Nanoplasmid before the 5′ end of the left homology arm via mutagenesis, synthesized, and the sequence verified (Cas9-CLIPT) (GenScript). Two other sequences with the *TRAC* sgRNA were designed in Benchling to contain additional transcripts encoding six NFAT response elements with minimal IL-2 promoter[49,50] to drive expression of an H2B-mCh reporter gene (Cas9-CLIPT NFAT-mCh) that was synthesized and the sequence verified (GenScript). All transgenes are flanked by 500-bp homology arms and were cloned into a pUC57 backbone. Plasmid products were shipped to Aldevron (Fargo, ND), where they were cloned into a Nanoplasmid backbone. Nanoplasmid backbones include two components: a small (∼300 bp) R6K origin of replication and an RNA-OUT cassette (∼70 bp). The latter encodes an antisense RNA that enables an antibiotic-free selection of *E. coli* cells in the presence of sucrose by preventing the expression of the genome-integrated levansucrase gene *sacB* and production of the toxic oligosaccharides from sucrose.[33] Nanoplasmids were manufactured using a proprietary *E. coli* fermentation process[29] and conventional DNA purification workflow. The latter applies the same methods for bacterial cell lysis, bacterial cell debris removal, chromatography, formulation, and DNA quality control as used for the "traditional" plasmids. Nanoplasmids were manufactured on-site at Aldevron and resuspended in DNase-free water at 2 mg/mL. Insert sequences can be found in Table S2.

Nanoplasmid linearization by restriction digest

To linearize Control Nanoplasmid for use as a dsDNA HDR template, a restriction digest of the Nanoplasmid construct using SspI-HF (catalog no. R3132S, New England Biolabs [NEB], Ipswich, MA) was performed. Four restriction digest batch reactions in 1.5-mL Eppendorf tubes (50 μL Nanoplasmid, 125 μL CutSmart buffer, 25 μL SspI-HF enzyme, and 1,050 μL DNase-free water for 1,250 μL total) were aliquoted (50 μL into PCR tubes for a total of 96 reactions). These were incubated in a thermocycler at 37°C for 15–60 min and heat inactivated at 65°C for 20 min according to the manufacturer's instructions. Gel electrophoresis was then performed on the finished product to assess whether proper cutting took place, followed by SPRI cleanups to purify and concentrate the material to 2 mg/mL. PCR reactions were pooled into eight 1.5-mL Eppendorf tubes (600 μL) with an equal volume of SPRI (Beckman Coulter, Brea, CA) beads that incubated for 5 min at room temperature. The product was washed twice with 70% ethanol and eluted in 75 μL DNase-free water and pooled into one tube (600 μL). This product was subject to a second round of cleanups and was eluted in 30 μL water. DNA was quantified using the NanoDrop2000 and Qubit dsDNA Broad Range (BR) Assay (Thermo Fisher Scientific) and diluted to 2 mg/mL according to Qubit measurements.

PCR-generated dsDNA HDR template production

Plasmids were used to make dsDNA PCR-generated donor template with tCTS adapters. This work was previously done,[17] but in brief, plasmids were MidiPrepped using the PureYield MidiPrep system (Promega, Madison, WI). PCR amplicons were generated from plasmid templates using Q5 Hot Start Polymerase (NEB) and pooled into 100-μL reactions for SPRI cleanup (1X) using AMPure XP beads according to the manufacturer's instructions (Beckman Coulter). Each 100 μL starting product was eluted into 5 μL water. Bead incubation and separation times were increased to 5 min, and elution time was increased to 15 min at 37°C to improve yield. PCR products from round 1 cleanup were pooled and subjected to a second round of SPRI cleanup (1X) to increase total concentration. The round 2 elution volume was 20% of the round 1 input volume. Template concentration and purity were quantified using NanoDrop 2000 and the Qubit dsDNA BR assay, and templates were diluted in water to an exact concentration of 2 μg/μL according to Qubit measurements.

Isolation of T cells from peripheral blood

Peripheral blood was drawn from healthy donors using an institutional review board-approved protocol (2018-0103). Blood was collected into lithium heparin-coated vacutainer tubes and transferred to 50 mL conical tubes. $CD3^+$ primary human T cells were isolated by negative selection per the manufacturer's instructions (catalog nos. 15021 and 15061, RosetteSep Human T Cell Enrichment Cocktail, STEMCELL Technologies, Vancouver, Canada). T cell pellets were resuspended in dilution medium (PBS with 2% FBS) and counted using a hemocytometer with 0.4% trypan blue viability stain (Thermo Fisher Scientific). Cells were then resuspended at 1 million/mL in TexMACS Cell Culture Medium (catalog no. 130-097-196, Miltenyi Biotec, Bergisch Gladbach, Germany). T cell cultures were supplemented with 10 ng/mL IL-7 (catalog no. 207-IL-005/CF, BioTechne, Minneapolis, MN) and 10 ng/mL IL-15 (catalog no. 247-ILB-005/CF, BioTechne) and stimulated with T cell TransAct (10 μL for each mL of culture, catalog no. 130-111-160, Miltenyi Biotec) for 72 h, respectively.

T cell EP on Lonza 4D-Nucleofector X Unit

Following T cell activation, the RNP and DNA were electroporated into T cells in 16-well EP cuvettes on a 4D-Nucleofector X Unit (catalog no. V4XP-3032, Lonza, Walkersville, VA) using pulse code EH-115. One million cells were electroporated per well in the cuvette. Per reaction, a *TRAC* locus-specific sgRNA (5′-CAGGGUUCUGG AUAUCUGU-3′) (IDT, Coralville, IA) (2 μL of 100 μM, IDT) was incubated with *Sp*Cas9 (0.8 μL of 10 mg/mL, catalog no. 9212-0.25MG, Aldevron) and PGA (15,000–50,000 kDa, 1.6 μL of 10 mg/mL solution in DNase free water, catalog no. 26247-79-0, Millipore Sigma, Burlington, MA) for 15 min at 37°C to form the RNP complex. During incubation, T cells were centrifuged at 300 *g* for 5 min and counted on the Countess II FL Automated Cell Counter (Thermo Fisher Scientific) with 0.4% trypan blue viability stain. One million cells per reaction were then aliquoted and centrifuged at 90 *g* for 10 min. Following RNP incubation, linearized dsDNA HDR templates were added to the mixtures (1 μL) in PCR tubes and incubated for at least 5 min. Cells were then resuspended in 18.6 μL P3 buffer (Lonza) and transferred to PCR tubes containing the RNP:DNA mixtures. Contents were then transferred to cuvettes (total volume 24 μL) and electroporated. Immediately following EP, 80 μL ImmunoCult-XF (catalog no. 10981, STEMCELL Technologies) with no cytokines was added to each reaction, which were then rested for 30 min at 37°C. Cells were then moved to a 96-well flat-bottom plate containing

160 μL medium supplemented with 10 ng/mL IL-7 (BioTechne), 10 ng/mL IL-15 (BioTechne), and 2.5 μM Nedisertib (M3814) (catalog no. S8586, Selleckchem, Houston, TX). Cells were cultured for 24 h and then transferred to 12-well plates with 1 mL media and incubated at 37°C for 48 h.

T cell EP on CEP system

Following T cell activation, RNPs and DNA were electroporated into T cells in the CEP cartridges (Cellares) using EP parameters co-developed with Cellares. For each at-scale reaction, 50 million cells were electroporated. Per reaction, an sgRNA (CAGGGUUCUGGA UAUCUGU) (IDT) specific for the *TRAC* locus (8.33 nmol, IDT) was incubated with *Sp*Cas9 (2.05 nmol, catalog no. 9212-0.25MG, Aldevron) for 15 min at 37°C to form the RNP complex. During incubation, T cells were counted on the NucleoCounter NC-200 (ChemoMetec, La Jolla, CA), aliquoted (50 million T cells per reaction), and centrifuged at 300 *g* for 10 min. Following RNP incubation, linearized dsDNA HDR templates were added to the mixtures (222 μg) in PCR tubes and incubated for at least 5 min. Cells were then resuspended in 1 mL Cellares EP Buffer, combined with the RNP:DNA mixtures, and transferred to the CEP chambers for EP. Cells were rested for 30 min at 37°C, then split into two wells of a G-Rex 6M Well Plate (catalog no. 80660M, Wilson Wolf, St. Paul, MN) containing 30 mL medium per well supplemented with 10 ng/mL IL-7 (BioTechne) and 10 ng/mL IL-15 (BioTechne). Cells were cultured for 3 days and then half the media was removed and replaced with fresh media. The cells were then incubated at 37°C for 48 h before being evaluated for editing efficiency.

T cell EP on Thermo Fisher Neon NxT EP system

Following T cell activation, the RNP and DNA were electroporated into T cells in Neon NxT 10 μL pipette tips (catalog no. N1025, Thermo Fisher Scientific) on a Neon NxT EP system (catalog no. NEON1S, Thermo Fisher Scientific) using pulse code 1600V/10ms/3. One million cells were electroporated per condition. Per reaction, a *TRAC* locus-specific sgRNA (5′-CAGGGUUCUG GAUAUCUGU-3′) (0.154 μL of 100 μM, IDT) was incubated with *Sp*Cas9 (0.2 μL of 10 mg/mL, catalog no. 9212-0.25MG, Aldevron) and PGA (0.123 μL of 10 mg/mL solution in DNase-free water, catalog no. 26247-79-0, Millipore Sigma) for 15 min at 37°C to form the RNP complex. During incubation, T cells were centrifuged at 300 *g* for 5 min and counted on the Countess II FL Automated Cell Counter (Thermo Fisher Scientific) with 0.4% trypan blue viability stain. One million cells per reaction were then aliquoted and centrifuged at 90 *g* for 10 min. Following RNP incubation, linearized dsDNA HDR templates were added to the mixtures (1 μL) in PCR tubes and incubated for at least 5 min. Cells were then resuspended in 10 μL genome editing buffer (Thermo Fisher Scientific) and transferred to PCR tubes containing the RNP:DNA mixtures. Contents were then transferred to Neon NxT 10 μL pipette tips and electroporated. Immediately following EP, 80 μL ImmunoCult-XF (catalog no. 10981, STEMCELL Technologies) with no cytokines was added to each reaction, which were then rested for 30 min at 37°C. Cells were then moved to a 96-well flat-bottom plate containing 160 μL medium supplemented with 10 ng/mL IL-7 (BioTechne), 10 ng/mL IL-15 (BioTechne), and 2.5 μM Nedisertib (M3814) (catalog no. S8586, Selleckchem). Cells were cultured for 24 h and then transferred to 12-well plates with 1 mL media and incubated at 37°C for 48 h.

T cell culture

TRAC-CAR T cells were cultured in TexMACS media supplemented with IL-7/IL-15 (10 ng/mL) at 1 million cells/mL for the first 3 days. After EP, *TRAC*-CAR T cells were cultured in ImmunoCult-XF for 7 days with IL-7/IL-15 (10 ng/mL). Every 2 days, cells were centrifuged at 300 *g* for 5 min and counted on the Countess II FL Automated Cell Counter with 0.4% trypan blue viability stain. Cells were then resuspended in culture medium at 1 million cells/mL. The same process was repeated on days 5 and 7 post-EP.

Flow cytometry analysis

CAR was detected using a 1A7 anti-14G2A antibody (National Cancer Institute, Biological Resources Branch, Bethesda, MD) conjugated to allophycocyanin (APC) using a Lightning Link APC Antibody Labeling kit (catalog no. 705-0010, Novus Biologicals, Centennial, CO). TCR was detected using an anti-human TCR α/β antibody conjugated to BV421 (catalog no. 306722, BioLegend). Flow cytometry to assess CAR and TCR positivity was performed on day 8 of manufacturing on an Attune NxT flow cytometer (Thermo Fisher Scientific). Immunophenotyping of cells was performed on day 10 of manufacturing using a spectral immunophenotyping panel on an Aurora spectral cytometer (Cytek, Cerritos, CA). Briefly, cells were plated in a 96-well round-bottom plate (100,000 cells for CAR/TCR and 250,000 cells for spectral immunophenotyping), washed with 200 μL PBS, and spun at 1,200 *g* for 1 min, twice. Cells were then stained for viability with either GhostRed 780 (catalog no. 50-105-2988, Tonbo Biosciences, San Diego, CA) or Live-Dead Blue (catalog no. L23105, Thermo Fisher Scientific). For CAR/TCR staining, 1 μL GhostRed 780 was added to 10 mL PBS to make a stock solution, and 100 μL stock solution was added to each sample and incubated for 30 min in the dark. For spectral flow staining, Live-Dead Blue stain was resuspended in 50 μL of DMSO, 1 μL added per 1 mL PBS to make a stock solution, and 200 μL stock solution was added to each sample and incubated for 30 min in the dark. After viability staining, samples were washed twice and blocked for 30 min with 50 μL fluorescence-activated cell sorting (FACS) buffer (0.5% BSA in PBS) with TruStain FcX solution (0.5 μL/sample, catalog no. 422301, BioLegend). Antibodies were then added to 100 μL BD Brilliant Stain Buffer (catalog no. 659611, BD Biosciences, Franklin Lakes, NJ) at the optimized amounts found in Table S3 and incubated for 1 h. Cells were then washed, resuspended in 200 or 75 μL FACS buffer, and analyzed on the Attune or Aurora, respectively. For spectral immunophenotyping, we used CD4, CD8, TCR, and CAR positivity to define populations, and for all markers, cells were gated by relative size, shape, singlets, viability, TCR negativity, and CAR transgene positivity to find an analyzable population of viable CAR T cells. All antibodies are listed in Table S3.

Stimulation of CAR T cells and flow cytometry

One million Cas9-CLIPT NFAT-mCh *TRAC*-CAR T cells were stimulated in 12-well plates with either PMA/ionomycin (10 ng/mL PMA, 1 μg/mL ionomycin) or 200,000 $GD2^+$ neuroblastoma CHLA-20 cells. Cells were counted and harvested after 24 h and stained for flow cytometry. Briefly, 100,000 cells were plated in a 96-well round-bottom plate, washed with 200 μL PBS, and spun at 1,200 *g* for 1 min twice. Cells were then stained for viability with GhostRed 780 and CAR in 100 μL of BD Brilliant Stain Buffer and incubated for 30 min in the dark. NFAT-mCh CAR T cells were stained for CAR and viability. Cells were then washed, resuspended in 75 μL FACS buffer, and analyzed on the Cytek Aurora instrument and were gated by relative size, shape, singlets, viability, TCR negativity, and CAR transgene positivity to find an analyzable population of viable CAR T cells. All antibodies are listed in Table S3.

In vitro cytotoxicity assay on IncuCyte

A total of 10,000 AkaLUC-GFP CHLA-20 cells were seeded in triplicate on 96-well plates and incubated for 24 h at 37°C. Twenty-four hours later, 100,000, 50,000, 25,000, 12,500, 6,250, or 3,130 CAR^+ T cells from day 10 of manufacturing were added to each well for E:T ratios of 10:1, 5:1, 2.5:1, 1.25:1, 0.625:1, or 0.313:1, respectively. The plate was centrifuged for 5 min at 100 *g* and then placed in the IncuCyte S3 Live-Cell Analysis System (Sartorius, Göttingen, Germany) and stored at 37°C in 5% CO_2. Images were taken every 3 h for 48 h. Green object count was used to calculate the number of cancer cells in each well, and fluorescent images were analyzed with IncuCyte Base Analysis software.

Spectral flow cytometry data analysis

Analysis of spectral flow cytometry data was performed using Cytek's SpectroFlo program. Single positive controls for each color were collected and analyzed in SpectroFlo for positive and negative populations. SpectroFlo's unmixing algorithm was then used to compensate for spillover and autofluorescence of cells. Data were then exported to FlowJo (version 10.9.0), where samples were gated for non-debris, singlets, and live cells. TCR and CAR positivity were used to gate cell populations for *in vitro* samples. Representative plots were generated in FlowJo using fluorescence minus one controls to set positive gates.

Linearization gel assays

TRAC sgRNA (1 μL of 100 μM) was incubated with *Sp*Cas9 (0.8 μL of 10 mg/mL) with or without PGA (1.6 μL of 10 mg/mL solution in DNase-free water) for 15 min at 37°C to form the RNP complex. To RNP complexes with and without PGA, Cas9-CLIPT or Control Nanoplasmid was added and incubated for 10 min. RNP:Nanoplasmid complexes were then run on a 1% agarose gel with a 1-kb ladder.

Data analysis and software

All data analyses were performed in GraphPad Prism (version 10.0.2) and Microsoft Excel. Statistical tests were done in GraphPad Prism and are indicated in the figure legends. Nanoplasmid sequences were designed in Benchling. FlowJo was used to analyze .fcs files exported from SpectroFlo and Attune NxT software. Representative flow plots were exported from FlowJo. Figures were created and organized using Adobe Illustrator (version 28.0). A p value less than 0.05 was defined as significant.

DNA extraction and PCR amplification

Genomic DNA was extracted from each sample using DNA QuickExtract (Lucigen, Middleton, WI) and the following program: 65°C for 15 min, 68°C for 15 min, and 98°C for 10 min. Amplicon primer sequences were designed in Benchling to flank the homology arms of the donor DNA templates. PCR was performed according to the manufacturer's instructions with Q5 Hot Start Polymerase (NEB) using the following programs for expected amplicon sizes: 3 kb amplicon: 98°C (30 s), 30 cycles of 98°C (10 s), 68°C (30 s), 72°C (1:30 min), and a final extension at 72°C (2 min); 6 kb amplicon: 98°C (30 s), 40 cycles of 98°C (10 s), 68°C (30 s), 72°C (5 min), and a final extension at 72°C (5 min). Forward primer: 5′-GGC CTTTTTCCCATGCCTGCCT-3′ and reverse primer: 5′-TGCCC TCTCCTGCCACCTTCTC-3′.

Oxford Nanopore Technologies sequencing

DNA concentration of PCR samples was quantified using NanoDrop 2000 and Qubit dsDNA BR assay (Thermo Fisher Scientific), and PCR samples were diluted in nuclease-free water to an exact concentration of 30 ng/μL according to Qubit measurements. Samples were sequenced on the Oxford Nanopore Technologies PromethION 24 according to the manufacturer's instructions. Prior to read alignment, the reference sequence was filtered from all non-IUPAC characters. All variants exhibiting a FILTER status of PASS are merged into the consensus sequence. Passing reads are sorted using a 2:1 weighted preference (length:quality), and the top 90% are kept for further analysis. QUAL is the Phred-scaled probability that the site has no variant and is computed as QUAL = −10*log10 (posterior genotype probability of a homozygous-reference genotype [GT = 0/0]). Analysis was performed using IGV and CRISPResso2 (crispresso2.pinellolab.org).

WGS for off-target sites

Genomic DNA was extracted from Cas9-CLIPT CAR T cells using the Gentra Puregene kit (Qiagen, Germantown, MD) per the manufacturer's instructions and quantified using Qubit. Samples were sequenced on the Oxford Nanopore Technologies PromethION 24 according to the manufacturer's instructions. WGS reads were aligned to the scFv region of the CAR transgene; reads with alignment to the transgene were subsequently mapped to the human genome (GRCh38). Mapping was performed with minimap2 utilizing the first half of the detectIS pipeline.[46,65,66] Reads were filtered for a minimum alignment length to chromosome or CAR of 150 bp and a minimum MAPQ value of 30. Integration sites were identified from reads aligning to both the transgene and the human genome filtered with an overlap window threshold (distance between the transgene aligning and the human genome aligning segments/total length of read) of 0.5.

DATA AVAILABILITY

Data are available upon request from the corresponding author, Krishanu Saha (ksaha@wisc.edu).

ACKNOWLEDGMENTS

We thank members of the Saha lab for experimental advice and the Capitini and Sodji labs for support at the facilities used. We also thank the University of Wisconsin Carbone Cancer Center Flow Cytometry Laboratory, supported by P30 CA014520, for use of its facilities and services, especially the Cytek Aurora Spectral Cytometer, "Pinky," supported by 1S10OD025225-01 (BD FACSymphony High Parameter Flow Cytometry). We thank Sarah Caroline-Gomes de Lima, Brookelyn Hrdlicka, and Alexandra McHale for helpful discussion and earlier optimization of manufacturing, and Matthew H. Forsberg for assistance setting up the co-culture potency assays.

We also acknowledge funding from NIH R01 CA278051, the National Science Foundation Engineering Research Center (ERC) for Cell Manufacturing Technologies (CMaT) NSF-EEC 1648035, the National Human Genome Research Institute Genomic Sciences Training Program T32HG002760, the University of Wisconsin (UW)-Madison Office of the Vice Chancellor for Research and Graduate Education with funding from the Wisconsin Alumni Research Foundation, Hyundai Hope on Wheels, the Grainger Institute for Engineering at UW-Madison, the St. Baldrick's Foundation Empowering Pediatric Immunotherapies for Childhood Cancers Team grant (C.M.C. and K.S.), the MACC Fund (C.M.C.), and NIH R35 GM119644-01 (K.S.). The contents of this article do not necessarily reflect the views or policies of the Department of Health and Human Services, nor does mention of trade names, commercial products, or organizations imply endorsement by the US government.

Aldevron and the Nanoplasmid product and service marks mentioned herein are trademarks or registered trademarks of Aldevron LLC in the United States and other countries. All other trademarks are the property of their respective owners.

AUTHOR CONTRIBUTIONS

D.C., A.T., and M.B. developed the restriction digest and two-step purification procedure for linearized HDR templates. K.L.-P. and H.S. performed the Nanoplasmid benchwork. D.A. designed the Nanoplasmid constructs and cloning workflows. J.A.W., S.R.P., and V.I. provided guidance and expertise for the Nanoplasmid platform and large-scale plasmid manufacturing. D.C., A.T., and M.B. optimized the EP protocols. D.C., A.T., and M.B. isolated and cultured T cells and performed virus-free transfections. D.C., A.T., and M.B. performed flow cytometry. D.C. and A.T. performed the *in vitro* co-cultures. D.C. and A.T. wrote the manuscript, with input from all authors. D.C., A.T., and M.B. performed the experiments and analyzed the data. S.Z.D. performed the WGS, K.G. processed and analyzed the WGS data, and M.M. supervised the WGS. A.T. worked with Cellares to implement Cas9-CLIPT on their automated platform. C.M.C. and K.S. supervised the research and edited the manuscript. D.C. led the drafting of the original manuscript. A.T. led the drafting of the revisions.

DECLARATION OF INTERESTS

A.T., D.C., M.B., K.L.-P., H.S., D.A., J.A.W., S.R.P., V.I., C.M.C., and K.S. are inventors on patents related to this work. K.L.-P., H.S., D.A., J.A.W., S.R.P., and V.I. are employed by Aldevron. Aldevron has patent rights covering Nanoplasmid product and technology, including US Patent Numbers 9,018,012, 9,109,012, 9,950,081, 9,550,998, 9,737,620, 10,047,365, 10,167,478, 10,844,388, 11,098,313, 11,851,665, and foreign equivalents thereof. C.M.C. receives honoraria for advisory board membership for Bayer, Nektar Therapeutics, and Novartis and has equity interest in and advisory board membership for Elephas. K.S. receives honoraria for advisory board membership for Andson Biotech, Notch Therapeutics, and Bharat Biotech.

SUPPLEMENTAL INFORMATION

Supplemental information can be found online at https://doi.org/10.1016/j.omtm.2025.101437.

REFERENCES

1. Hashmi, H., Hansen, D.K., Peres, L.C., Puglianini, O.C., Freeman, C., De Avila, G., Sidana, S., Shune, L., Sborov, D.W., Davis, J., et al. (2024). Factors associated with refractoriness or early progression after idecabtagene vicleucel in patients with relapsed/refractory multiple myeloma: US Myeloma Immunotherapy Consortium real world experience. Haematologica *109*, 1514–1524.
2. Chen, Y.-J., Abila, B., and Mostafa Kamel, Y. (2023). CAR-T: What Is Next? Cancers *15*, 663.
3. Keam, S.J. (2024). Afamitresgene Autoleucel: First Approval. Mol. Diagn. Ther. *28*, 861–866.
4. Zheng, P.-P., Kros, J.M., and Li, J. (2018). Approved CAR T cell therapies: ice bucket challenges on glaring safety risks and long-term impacts. Drug Discov. Today *23*, 1175–1182.
5. KYMRIAH® (tisagenlecleucel). https://www.us.kymriah.com/.
6. Rotte, A., Frigault, M.J., Ansari, A., Gliner, B., Heery, C., and Shah, B. (2022). Dose-response correlation for CAR-T cells: a systematic review of clinical studies. J. Immunother. Cancer *10*, e005678.
7. Patel, R., Gurumurthi, A., Feng, L., Westin, J., Nastoupil, L.J., Nair, R., Iyer, S.P., Torres, J.M., Nieto, Y., Kebriaei, P., et al. (2024). Factors associated with manufacturing failure of commercial CD19 CAR-T cell products for large b cell lymphoma (LBCL). J. Clin. Oncol. *42*, 7044. https://doi.org/10.1200/JCO.2024.42.16_suppl.7044.
8. CAR-T Cell Therapy Program. Mayo Clinic. https://www.mayoclinic.org/departments-centers/car-t-cell-therapy-program/sections/gnc-20405547.
9. Baker, D.J., Arany, Z., Baur, J.A., Epstein, J.A., and June, C.H. (2023). CAR T therapy beyond cancer: the evolution of a living drug. Nature *619*, 707–715.
10. Levine, B.L., Pasquini, M.C., Connolly, J.E., Porter, D.L., Gustafson, M.P., Boelens, J.J., Horwitz, E.M., Grupp, S.A., Maus, M.V., Locke, F.L., et al. (2024). Unanswered questions following reports of secondary malignancies after CAR-T cell therapy. Nat. Med. *30*, 338–341.
11. Zhang, J., Hu, Y., Yang, J., Li, W., Zhang, M., Wang, Q., Zhang, L., Wei, G., Tian, Y., Zhao, K., et al. (2022). Non-viral, specifically targeted CAR-T cells achieve high safety and efficacy in B-NHL. Nature *609*, 369–374.
12. Ghosh, S., Brown, A.M., Jenkins, C., and Campbell, K. (2020). Viral Vector Systems for Gene Therapy: A Comprehensive Literature Review of Progress and Biosafety Challenges. Appl. Biosaf. *25*, 7–18.
13. Cong, L., Ran, F.A., Cox, D., Lin, S., Barretto, R., Habib, N., Hsu, P.D., Wu, X., Jiang, W., Marraffini, L.A., and Zhang, F. (2013). Multiplex genome engineering using CRISPR/Cas systems. Science *339*, 819–823.
14. Mali, P., Yang, L., Esvelt, K.M., Aach, J., Guell, M., DiCarlo, J.E., Norville, J.E., and Church, G.M. (2013). RNA-guided human genome engineering via Cas9. Science *339*, 823–826.
15. Wang, Z., Li, N., Feng, K., Chen, M., Zhang, Y., Liu, Y., Yang, Q., Nie, J., Tang, N., Zhang, X., et al. (2021). Phase I study of CAR-T cells with PD-1 and TCR disruption in mesothelin-positive solid tumors. Cell. Mol. Immunol. *18*, 2188–2198.
16. Eyquem, J., Mansilla-Soto, J., Giavridis, T., van der Stegen, S.J.C., Hamieh, M., Cunanan, K.M., Odak, A., Gönen, M., and Sadelain, M. (2017). Targeting a CAR to the TRAC locus with CRISPR/Cas9 enhances tumour rejection. Nature *543*, 113–117.
17. Mueller, K.P., Piscopo, N.J., Forsberg, M.H., Saraspe, L.A., Das, A., Russell, B., Smerchansky, M., Cappabianca, D., Shi, L., Shankar, K., et al. (2022). Production and characterization of virus-free, CRISPR-CAR T cells capable of inducing solid tumor regression. J. Immunother. Cancer *10*, e004446.
18. Roth, T.L., Puig-Saus, C., Yu, R., Shifrut, E., Carnevale, J., Li, P.J., Hiatt, J., Saco, J., Krystofinski, P., Li, H., et al. (2018). Reprogramming human T cell function and specificity with non-viral genome targeting. Nature *559*, 405–409.
19. Biasco, L., Izotova, N., Rivat, C., Ghorashian, S., Richardson, R., Guvenel, A., Hough, R., Wynn, R., Popova, B., Lopes, A., et al. (2021). Clonal expansion of T memory stem cells determines early anti-leukemic responses and long-term CAR T cell persistence in patients. Nat. Cancer *2*, 629–642.
20. Prather, K.J., Sagar, S., Murphy, J., and Chartrain, M. (2003). Industrial scale production of plasmid DNA for vaccine and gene therapy: plasmid design, production, and purification. Enzyme Microb. Technol. *33*, 865–883.
21. Listner, K., Bentley, L., Okonkowski, J., Kistler, C., Wnek, R., Caparoni, A., Junker, B., Robinson, D., Salmon, P., Chartrain, M., et al. (2006). Development of a highly productive and scalable plasmid DNA production platform. Biotechnol. Prog. *22*, 1335–1345.

22. Jing, R., Jiao, P., Chen, J., Meng, X., Wu, X., Duan, Y., Shang, K., Qian, L., Huang, Y., Liu, J., et al. (2021). Cas9-Cleavage Sequences in Size-Reduced Plasmids Enhance Nonviral Genome Targeting of CARs in Primary Human T Cells. Small Methods *5*, e2100071.

23. Oh, S.A., Senger, K., Madireddi, S., Akhmetzyanova, I., Ishizuka, I.E., Tarighat, S., Lo, J.H., Shaw, D., Haley, B., and Rutz, S. (2022). High-efficiency nonviral CRISPR/Cas9-mediated gene editing of human T cells using plasmid donor DNA. J. Exp. Med. *219*, e20211530.

24. Hu, Y., Zu, C., Zhang, M., Wei, G., Li, W., Fu, S., Hong, R., Zhou, L., Wu, W., Cui, J., et al. (2023). Safety and efficacy of CRISPR-based non-viral PD1 locus specifically integrated anti-CD19 CAR-T cells in patients with relapsed or refractory Non-Hodgkin's lymphoma: a first-in-human phase I study. EClinicalMedicine *60*, 102010.

25. Shy, B.R., Vykunta, V.S., Ha, A., Talbot, A., Roth, T.L., Nguyen, D.N., Pfeifer, W.G., Chen, Y.Y., Blaeschke, F., Shifrut, E., et al. (2023). High-yield genome engineering in primary cells using a hybrid ssDNA repair template and small-molecule cocktails. Nat. Biotechnol. *41*, 521–531.

26. Nguyen, D.N., Roth, T.L., Li, P.J., Chen, P.A., Apathy, R., Mamedov, M.R., Vo, L.T., Tobin, V.R., Goodman, D., Shifrut, E., et al. (2020). Polymer-stabilized Cas9 nanoparticles and modified repair templates increase genome editing efficiency. Nat. Biotechnol. *38*, 44–49.

27. Lei, L., Chen, H., Xue, W., Yang, B., Hu, B., Wei, J., Wang, L., Cui, Y., Li, W., Wang, J., et al. (2018). APOBEC3 induces mutations during repair of CRISPR–Cas9-generated DNA breaks. Nat. Struct. Mol. Biol. *25*, 45–52.

28. Seyed, N., Zahedifard, F., Habibzadeh, S., Yousefi, R., Lajevardi, M.S., Gholami, E., and Rafati, S. (2022). Antibiotic-Free Nanoplasmids as Promising Alternatives for Conventional DNA Vectors. Vaccines (Basel) *10*, 1710.

29. Carnes, A., Tiwari, N., Beilowitz, J., Sampson, C., Peterson, D., and Williams, J. (2016). Production of a Nanoplasmid™ with a large gene insert using the HyperGRO™ fermentation process. In Vaccine Technology VI. ECI Symposium Series, L. Palomares, M. Cox, T. Mukhopadhyay, and N. Garçon, eds. http://dc.engconfintl.org/vaccine_vi/77.

30. Suschak, J.J., Dupuy, L.C., Shoemaker, C.J., Six, C., Kwilas, S.A., Spik, K.W., Williams, J.A., and Schmaljohn, C.S. (2020). Nanoplasmid Vectors Co-expressing Innate Immune Agonists Enhance DNA Vaccines for Venezuelan Equine Encephalitis Virus and Ebola Virus. Mol. Ther. Methods Clin. Dev. *17*, 810–821.

31. Ostertag, E. (2020). Manufacturing Matters in CAR T. https://poseida.com/wp-content/uploads/2021/01/Manufacturing-Matters-in-CAR-T.pdf.

32. Moretti, A., Ponzo, M., Nicolette, C.A., Tcherepanova, I.Y., Biondi, A., and Magnani, C.F. (2022). The Past, Present, and Future of Non-Viral CAR T Cells. Front. Immunol. *13*, 867013.

33. Williams, J.A., and Paez, P.A. (2023). Improving cell and gene therapy safety and performance using next-generation Nanoplasmid vectors. Mol. Ther. Nucleic Acids *32*, 494–503.

34. Yao, X., Wang, X., Hu, X., Liu, Z., Liu, J., Zhou, H., Shen, X., Wei, Y., Huang, Z., Ying, W., et al. (2017). Homology-mediated end joining-based targeted integration using CRISPR/Cas9. Cell Res. *27*, 801–814.

35. Wierson, W.A., Welker, J.M., Almeida, M.P., Mann, C.M., Webster, D.A., Torrie, M.E., Weiss, T.J., Kambakam, S., Vollbrecht, M.K., Lan, M., et al. (2020). Efficient targeted integration directed by short homology in zebrafish and mammalian cells. Elife *9*, e53968.

36. Balke-Want, H., Keerthi, V., Gkitsas, N., Mancini, A.G., Kurgan, G.L., Fowler, C., Xu, P., Liu, X., Asano, K., Patel, S., et al. (2023). Homology-independent targeted insertion (HITI) enables guided CAR knock-in and efficient clinical scale CAR-T cell manufacturing. Mol. Cancer *22*, 100.

37. Webber, B.R., Johnson, M.J., Skeate, J.G., Slipek, N.J., Lahr, W.S., DeFeo, A.P., Mills, L.J., Qiu, X., Rathmann, B., Diers, M.D., et al. (2024). Cas9-induced targeted integration of large DNA payloads in primary human T cells via homology-mediated end-joining DNA repair. Nat. Biomed. Eng. *8*, 1553–1570. https://doi.org/10.1038/s41551-023-01157-4.

38. Arai, D., and Nakao, Y. (2021). Efficient biallelic knock-in in mouse embryonic stem cells by *in vivo*-linearization of donor and transient inhibition of DNA polymerase θ/DNA-PK. Sci. Rep. *11*, 18132.

39. Tumaini, B., Lee, D.W., Lin, T., Castiello, L., Stroncek, D.F., Mackall, C., Wayne, A., and Sabatino, M. (2013). Simplified process for the production of anti-CD19-CAR-engineered T cells. Cytotherapy *15*, 1406–1415.

40. Balke-Want, H., Keerthi, V., Cadinanos-Garai, A., Fowler, C., Gkitsas, N., Brown, A.K., Tunuguntla, R., Abou-El-Enein, M., and Feldman, S.A. (2023). Non-viral chimeric antigen receptor (CAR) T cells going viral. Immunooncol. Technol. *18*, 100375.

41. Cappabianca, D., Pham, D., Forsberg, M.H., Bugel, M., Tommasi, A., Lauer, A., Vidugiriene, J., Hrdlicka, B., McHale, A., Sodji, Q.H., et al. (2024). Metabolic priming of GD2 TRAC-CAR T cells during manufacturing promotes memory phenotypes while enhancing persistence. Mol. Ther. Methods Clin. Dev. *32*, 101249.

42. Pham, D.L., Cappabianca, D., Forsberg, M.H., Weaver, C., Mueller, K.P., Tommasi, A., Vidugiriene, J., Lauer, A., Sylvester, K., Bugel, M., et al. (2024). Label free metabolic imaging to enhance the efficacy of Chimeric Antigen Receptor T cell therapy. Preprint at bioRxiv. https://doi.org/10.1101/2024.02.20.581240.

43. Fu, Y.-W., Dai, X.-Y., Wang, W.-T., Yang, Z.-X., Zhao, J.-J., Zhang, J.-P., Wen, W., Zhang, F., Oberg, K.C., Zhang, L., et al. (2021). Dynamics and competition of CRISPR-Cas9 ribonucleoproteins and AAV donor-mediated NHEJ, MMEJ and HDR editing. Nucleic Acids Res. *49*, 969–985.

44. Marx, V. (2023). Method of the year: long-read sequencing. Nat. Methods *20*, 6–11.

45. Acinas, S.G., Sarma-Rupavtarm, R., Klepac-Ceraj, V., and Polz, M.F. (2005). PCR-Induced Sequence Artifacts and Bias: Insights from Comparison of Two 16S rRNA Clone Libraries Constructed from the Same Sample. Appl. Environ. Microbiol. *71*, 8966–8969.

46. Guo, C., Ma, X., Gao, F., and Guo, Y. (2023). Off-target effects in CRISPR/Cas9 gene editing. Front. Bioeng. Biotechnol. *11*, 1143157.

47. Mikocziova, I., Greiff, V., and Sollid, L.M. (2021). Immunoglobulin germline gene variation and its impact on human disease. Genes Immun. *22*, 205–217.

48. Six, E.M., Benjelloun, F., Garrigue, A., Bonhomme, D., Morillon, E., Rouiller, J., Cacavelli, L., Blondeau, J., Beldjord, K., Hacein-Bey-Abina, S., et al. (2011). Cytokines and culture medium have a major impact on human *in vitro* T-cell differentiation. Blood Cells Mol. Dis. *47*, 72–78.

49. Liu, Y., Di, S., Shi, B., Zhang, H., Wang, Y., Wu, X., Luo, H., Wang, H., Li, Z., and Jiang, H. (2019). Armored Inducible Expression of IL-12 Enhances Antitumor Activity of Glypican-3-Targeted Chimeric Antigen Receptor-Engineered T Cells in Hepatocellular Carcinoma. J. Immunol. *203*, 198–207.

50. Rooney, J.W., Sun, Y.L., Glimcher, L.H., and Hoey, T. (1995). Novel NFAT sites that mediate activation of the interleukin-2 promoter in response to T-cell receptor stimulation. Mol. Cell Biol. *15*, 6299–6310.

51. Macian, F. (2005). NFAT proteins: key regulators of T-cell development and function. Nat. Rev. Immunol. *5*, 472–484.

52. Zhang, S., Shen, J., Li, D., and Cheng, Y. (2021). Strategies in the delivery of Cas9 ribonucleoprotein for CRISPR/Cas9 genome editing. Theranostics *11*, 614–648.

53. Gehl, J. (2003). Electroporation: theory and methods, perspectives for drug delivery, gene therapy and research. Acta Physiol. Scand. *177*, 437–447.

54. Ma, Y., Poole, K., Goyette, J., and Gaus, K. (2017). Introducing Membrane Charge and Membrane Potential to T Cell Signaling. Front. Immunol. *8*, 1513.

55. Zhang, J.-P., Li, X.-L., Li, G.-H., Chen, W., Arakaki, C., Botimer, G.D., Baylink, D., Zhang, L., Wen, W., Fu, Y.-W., et al. (2017). Efficient precise knockin with a double cut HDR donor after CRISPR/Cas9-mediated double-stranded DNA cleavage. Genome Biol. *18*, 35.

56. Suzuki, K., Tsunekawa, Y., Hernandez-Benitez, R., Wu, J., Zhu, J., Kim, E.J., Hatanaka, F., Yamamoto, M., Araoka, T., Li, Z., et al. (2016). In vivo genome editing via CRISPR/Cas9 mediated homology-independent targeted integration. Nature *540*, 144–149.

57. Selvaraj, S., Feist, W.N., Viel, S., Vaidyanathan, S., Dudek, A.M., Gastou, M., Rockwood, S.J., Ekman, F.K., Oseghale, A.R., Xu, L., et al. (2024). High-efficiency transgene integration by homology-directed repair in human primary cells using DNA-PKcs inhibition. Nat. Biotechnol. *42*, 731–744.

58. Samulski, R.J., and Muzyczka, N. (2014). AAV-Mediated Gene Therapy for Research and Therapeutic Purposes. Annu. Rev. Virol. *1*, 427–451.

59. Wang, D., Tai, P.W.L., and Gao, G. (2019). Adeno-associated virus vector as a platform for gene therapy delivery. Nat. Rev. Drug Discov. *18*, 358–378.

60. Ye, L., Park, J.J., Peng, L., Yang, Q., Chow, R.D., Dong, M.B., Lam, S.Z., Guo, J., Tang, E., Zhang, Y., et al. (2022). A genome-scale gain-of-function CRISPR screen in CD8 T cells identifies proline metabolism as a means to enhance CAR-T therapy. Cell Metab. *34*, 595–614.e14.

61. Doan, A.E., Mueller, K.P., Chen, A.Y., Rouin, G.T., Chen, Y., Daniel, B., Lattin, J., Markovska, M., Mozarsky, B., Arias-Umana, J., et al. (2024). FOXO1 is a master regulator of memory programming in CAR T cells. Nature *629*, 211–218.

62. Chan, J.D., Scheffler, C.M., Munoz, I., Sek, K., Lee, J.N., Huang, Y.-K., Yap, K.M., Saw, N.Y.L., Li, J., Chen, A.X.Y., et al. (2024). FOXO1 enhances CAR T cell stemness, metabolic fitness and efficacy. Nature *629*, 201–210.

63. Allen, G.M., Frankel, N.W., Reddy, N.R., Bhargava, H.K., Yoshida, M.A., Stark, S.R., Purl, M., Lee, J., Yee, J.L., Yu, W., et al. (2022). Synthetic cytokine circuits that drive T cells into immune-excluded tumors. Science *378*, eaba1624.

64. Kwon, J., Kang, J., Jo, A., Seo, K., An, D., Baykan, M.Y., Lee, J.H., Kim, N., Eum, H.H., Hwang, S., et al. (2023). Single-cell mapping of combinatorial target antigens for CAR switches using logic gates. Nat. Biotechnol. *41*, 1593–1605.

65. Li, H. (2018). Minimap2: pairwise alignment for nucleotide sequences. Bioinformatics *34*, 3094–3100.

66. Grassi, L., Harris, C., Zhu, J., Hardman, C., and Hatton, D. (2021). DetectIS: a pipeline to rapidly detect exogenous DNA integration sites using DNA or RNA paired-end sequencing data. Bioinformatics *37*, 4230–4232.